INSTITUTO SUPERIOR TÉCNICO
Universidade Técnica de Lisboa

TRANSIENT ANALYSIS AND EVALUATION IN RECONFIGURABLE OPTICAL NETWORKS

Pedro Miguel Vieira Duarte

Dissertation submitted for obtaining the degree of Master in Electrical and Computer Engineering

President: Prof. António J. Rodrigues
Supervisor: Prof. António L. Topa
Co-Supervisor: Dr. Ruben Luís
Member: Prof. Adolfo Cartaxo

Setembro de 2008

Acknowledgements

The conclusion of the work reported in the present dissertation was attained thanks to the contribution of several persons, in many different ways.

I wish to express my thanks to Ruben Luís for his careful, supervision, advice, motivation, useful explanations and also Álvaro Buxens for allowing me the possibility of working in such an interesting subject. I am also thankful to Professor António Topa for his continuous presence throughout this study.

To Nokia Siemens Networks S.A. for providing pleasant working conditions, and in particular to, my colleagues, I express my gratitude for the excellent work environment, interesting discussions, constant availability to provide important elucidations.

A special thanks to Diana for her permanent and unconditional support, motivation and affection. To my parents, all my family and friends, I am grateful for their care and attention.

Thank you all!

Abstract

The next-generation of optical network systems provide the ability to remotely configure which wavelengths are added/dropped, or expressed through a node. The enabling of this technology has several tradeoffs. One of the impacts of using re-configurable wavelength routing is the transient response of the optical amplifiers to abrupt changes of the input power. These abrupt add/drops result in fluctuations in the power of each channel producing significant optical power transients that propagate along the optical amplifiers throughout the network, causing severe performance degradation.

An analytical model was implemented to simulate the transient propagation in optical links and evaluate the impacts on the link optical performance. Several parameters are defined to characterize a power transient response and limits to these parameters are imposed.

Finally, an experimental analysis of an amplifier chain is performed and the simulation results are qualitatively demonstrated.

Keywords: *DWDM* reconfigurable optical networks, amplifiers dynamic response, transients.

Resumo

A próxima geração de redes ópticas permitirá configurar remotamente que canais são adicionados/removidos ou redireccionados através de um determinado nó da rede. A implementação desta tecnologia possui alguns compromissos. Um dos impactos de redes ópticas reconfigurávies é a resposta transitória dos amplificadores ópticos. Adicionar e remover canais provoca fluctuações abruptas da potência à entrada dos amplificadores o que resulta em respostas transitórias na potência de cada canal à saída. Estas flutuações propagam-se ao longo dos amplificadores ópticos de toda a rede, o que resulta numa degradação do desempenho.

Um modelo analítico de um Amplificador de Fibra Dopada de Érbio foi implementado para simular a propagação de regimes transitórios de potência em caminhos ópticos e avaliar os impactos no desempenho óptico. São definidos vários parâmetros com o objectivo de caracterizar uma resposta transitória de potência e são impostos limites para estes parametros.

Por último, uma análise experimental de amplificadores ópticos em cadeia é realizada e os resultados simulados são qualitativamente demonstrados.

Palavras-Chave: Redes Ópticas Reconfiguráveis, Resposta Transitória de Amplificadores de Fibra Dopada de Érbio.

Table of Contents

List of Figures

List of Tables

List of Acronyms

AGC	Automatic Gain Control
APD	Avalanche Photo Diode
ASE	Amplified Spontaneous Emission
AWG	Arrayed Waveguide Gratting
BER	Bit Error Ratio
CW	Continuous Wave
DSF	Dispersion-Shifted Fiber
DWDM	Dense-Wavelength Division Multiplex
ECL	External Cavity Laser
EDFA	Erbium-Doped Fiber Amplifier
FEC	Forward Error Correction
FTTP	Fiber To The Premises
FWM	Four-Wave Mixing
MZ	Mach-Zhender
NF	Noise Figure
NRZ	Non-Return-to-Zero
OLT	Optical Line Terminal
ON	Optical Node
OSA	Optical Spectrum Analyser
OSNR	Optical Signal-to-Noise Ratio
OXC	Optical cross-Connect
PON	Passive Optical Network
POP	Point Of Presence
ROADM	Reconfigurable Optical Add and Drop Multiplexer
SDH	Synchronous Digital Hierarchy
SPM	Self Phase Modulation
VOA	Variable Optical Attenuator
WDM	Wavelength Division Multiplexing
WRON	Wavelength Routed Optical Network
XPM	Cross Phase Modulation
ODE	Ordinary Differential Equation

List of Symbols

A_{eff}	Effective Area of the Fiber Core
A_j	Adimensional Parameter
Att	Attenuation
B_e	Electrical Filter
B_j	Adimensional Parameter
B_o	Optical Filter
f	Optical Signal Frequency
G	Gain
h	Planck's Constant
L	Amplifier Length.
m	Number of *EDFA*s
mp	Undershoot
Mp	Overshoot
N	Number of Channels
$OSNRe_{tr}$,	*OSNR* Excursion at Rise/Fall time
$OSNRe_{tp}$,	*OSNR* Excursion at Peak Time
$OSNRe_{mp}$	*OSNR* Excursion at Undershoot Instant
$OSNRe_{ts}$	*OSNR* Excursion at Settling Time
P	Power
Pe	Power Excursion
Pe_{mp}	Power Excursion at Undershoot Instant
Pe_{tp}	Power Excursion at Peak Time
Pe_{tr}	Power Excursion at Rise/Fall time
Pe_{ts}	Power Excursion at Settling Time
$Pe(tr)_{drop}$	Power Excursion at Instant *tr* After a Channel Drop
P_{in}	Input Power
$P^{in}_{j,1}$	Power per Channel j at the Input of the First *EDFA*
P^{in}_{m}	Input Power at the m^{th} *EDFA*
P_j^{IS}	Intrinsic Saturation Power
P^{N}_{m}	Noise Power at the Input of the m^{th} EDFA

P_{out}	Output Power
P_{out}^{total}	Total Output Power
$P^{out}{}_{m}$	Output Power at the m^{th} *EDFA*
Pp	Pump Power
Q	Photon flux
Qe_{mp}	Q-factor Excursion at Undershoot Instant
Qe_{tp},	Q-factor Excursion at Peak Time
Qe_{tr},	Q-factor Excursion at Rise/Fall time
$Qe_{ts.}$	Q-factor Excursion at Settling Time
Q_j^{in}	Photon Flux per Channel at the Input
Q_j^{out}	Photon Flux per Channel j at the Output
r	Reservoir, Number of excited ions.
r_M	Total Number of Ions in the Doped Fiber
SR	Slew Rate
tp	Peak time
tr	Rise time/Fall time
ts	Settling time
Δf	Reference Bandwidth for the Noise Measurement,
α_j	Absorption Coefficient
λ_1	Channel Number 1
λ_N	Channel Number N
ρ	Ions density
σ_j^e	Emission Cross-Section of Channel j
σ_j^a	Absorption Cross-Section of Channel j
τ	Fluorescence Time
Γ_j	Confinement Factor

Chapter 1. Introduction

1.1 Introduction

The present chapter has as main goal to give a global perspective of the problem in study. The problem under analysis is the transient dynamics in Erbium-Doped Fiber Amplifiers (*EDFA*s) gain and power after an abrupt change of the input power, and its consequences in Dense Wavelength Division Multiplexing (*DWDM*) optical networks. The importance of transients study in today's optical networks is presented. A description of the thesis content and structure is also presented. The chapter ends with the novel contributions.

1.2 Motivation

Over the past decade, the field of telecommunications has experienced an enormous growth. This fact is due to the rapidly growth of the internet and the world wide web. The work of Borella *et al.* in [1] presented that a near future may bring multiple connections of high-definition television, video mail, and digital audio, as well as full internet connections via user-friendly graphic interfaces. Approximately ten years later this scenario starts to become a reality. As more users start to use data networks, and as their networking applications include more bandwidth needs, there emerges a growing need for very high bandwidth transport network facilities. The capabilities and flexibility of such facilities in delivering a variable bandwidth according to service providers demands, greatly exceeds the high-speed networks, such as Synchronous Digital Hierarchy (*SDH*) networks [1].

The key to the future of networks rests in the field of optical networks [1]. The maturity of this technology is well reflected by the accelerated rate at which optical fiber links are currently being deployed over the continents and across the oceans. The progress can be measured by considering that, in 1993, the existing transoceanic fiber links based on digital communications techniques could transmit 40 000 to 80 000 simultaneous telephone conversations, as compared to 36 in the first telephone cable deployed in 1956 between the United Kingdom and the United States [2]. For

example, the highest capacity of commercial fiber-optic links available in 1992 was only 2.5 Gb/s. A mere 4 years later, the wavelength-division-multiplexed (*WDM*) systems with the total capacity of 40Gb/s became available commercially. By 2001, the capacity of commercial *WDM* systems exceeded 1.6Tb/s, and prospect of commercial lightwave systems operating at 3.2 Tb/s are in sight [3].

Optical fiber provides huge bandwidth, low loss rate, and cost effectiveness [1]. The limits imposed by the use of this transmission mean are yet to be found. Using wavelengths on a bandwidth around 1.3μm and 1.55μm it offers a comfortable bandwidth of 45THz, still largely underused [2]. The use of *WDM* systems is one approach to exploit effectively the huge bandwidth of optical fibers. In *WDM*, the optical transmission spectrum is divided into a number of nonoverlapping wavelength (or frequency) bands, with each wavelength supporting a single communication channel operating at a determinate traffic rate (10Gb/s, 40Gb/s commercially available). Thus, by allowing multiple *WDM* channels to coexist on a single fiber, one may tap into the huge fiber bandwidth [1], [4]. The number of channels in which the spectrum can be divided is variable. Nowadays, the use of 50 GHz spacing commercially is very common and these systems are called *DWDM* [5].

The high-capacity transport networks of the future need to grow on dimensions and complexity of the electronic switches and cross-connects, becoming unbearable from an economic point of view [6]. In this context, the need to regenerate optical signals as they undergo attenuation and loss when propagating along a fiber link or network, constitute a real limitation in optical networks. The task of signal regeneration traditionally has been performed by electronic regenerators, in which optical signals are converted into the electric domain, regenerated and then converted back into light. Regenerators must be placed at intervals such that the optical signal power never drops below a level where the probability of misreading digital symbols becomes unacceptably high. As an example, in 1993, transatlantic fiber links typically had 70 km regenerator spacing, which are about 100 regenerators over their 7500 km length. Another drawback of electronic regeneration is that *WDM* implementation is difficult and costly. This is because many parallel regenerators are needed to combine several optical channels into the same fiber [2].

A major milestone in the evolution of optical fiber transmission systems was the development of optical amplifiers, such as Raman amplifiers and *EDFA*s. A major advantage of optical amplifiers is that they are capable of amplifying signals at many wavelengths simultaneously. The use of *WDM* and optical amplifiers dramatically brought down the cost of long-haul transmission systems and increased their capacity. Thus, although an optical signal can propagate a long distance before it needs amplification, both long-haul and local lightwave networks can benefit from optical amplifiers. All-optical amplification may differ from optoelectronic regeneration in that it may act only to boost the power of a signal, not to restore the shape or timing of signal. This type of amplification provides total data transparency (the amplification process is independent of signal's modulation format), being the emerging choice for the transparent all-optical networks of tomorrow [1], [4].

Optical amplifiers such as *EDFA*s can be designed to operate over the spectral range of either the C- or L-band. *EDFA*s use a short length of erbium-doped fiber as the gain medium. A typical *EDFA* supports 80-90 wavelengths within 50GHz spacing or 40-50 within 100GHz spacing in the C-band (1530 – 1565 nm). This has allowed a single amplifier to replace per wavelength optoelectronic regenerators in today's *DWDM* systems thus significantly reducing cost. Stimulated Raman Scattering (*SRS*) can also be used to provide amplification. *SRS* is typically used to implement distributed amplification in the transmission fiber although discrete implementations, using dispersion compensating fiber are also being used. Raman amplification uses high-power lasers pumps with a wavelength approximately 100 nm shorter than the wavelength signal to be amplified. This allows Raman amplification to be implemented at any signal wavelength by selecting a suitable pump wavelength. Raman amplifiers can also operate over a wider band than *EDFA*s but generally require more pump lasers with high output power. *EDFA*s and Raman amplifiers can be combined to maximize performance especially in long-haul applications. Unfortunately, the use of optical amplification is accompanied by the generation of amplifier noise, referred to as amplified spontaneous emission (*ASE*). The noise contributions of each in-line optical amplifier in a transmission system add cumulatively and are characterized by the amplifier's noise figure (*NF*). In *ASE*-limited systems, the noise in the receiver is quantified as the optical signal-to-noise ratio (*OSNR*). Defined as the ratio of the optical signal power to the *ASE* power in a

specific optical bandwidth (usually taken to be 0.1 nm), *OSNR* is the dominant factor determining the receiver bit error ratio (*BER*). The required *OSNR* for a specific *BER* can be significantly reduced through the use of forward error correction (*FEC*). It is important to distinguish the *BER* at the receiver, which is related to the *OSNR* and the *BER* after *FEC*. The *BER* after *FEC* represents the amount of errors that are uncorrectable and pass to clients. The use of *FEC* allows the receiver to operate at a much higher *BER* than the specified target *BER* for the system.

Telecommunication networks are usually segmented into a three level hierarchy: access, metropolitan and long-haul [7]. Long-haul networks cover inter-regional distances (1000 km or more) and allow a large tributary connectivity between regional and metropolitan [1] domains. On the opposite side of this hierarchy are access networks. The last few years have seen increasing deployment of access technologies such as fiber to the premises (*FTTP*). The bandwidth requirements of today users drive the requirements for a new generation of *DWDM* networks and the extension of such networks into areas that previously did not require *DWDM* technology. Past *DWDM* metropolitan deployments have focused on small rings of three to six nodes. A new architecture must evolve to support mesh clusters of 20-50 nodes in a metropolitan area. Multiwavelength *DWDM* networks have evolved from simple point-to-point systems to linear chains and rings, and are now changing to generalized mesh topologies. Figure 1-1 illustrates a typical *DWDM* transport network where is represented common topologies such the ring, mesh, and a point-to-point link. It also exhibits some possible *clients* of a *DWDM* network: access networks such as *PON*s (Passive Optical Networks), data centres, enterprises, etc.

[1] Metropolitan Networks are commonly referred to by Metro Networks.

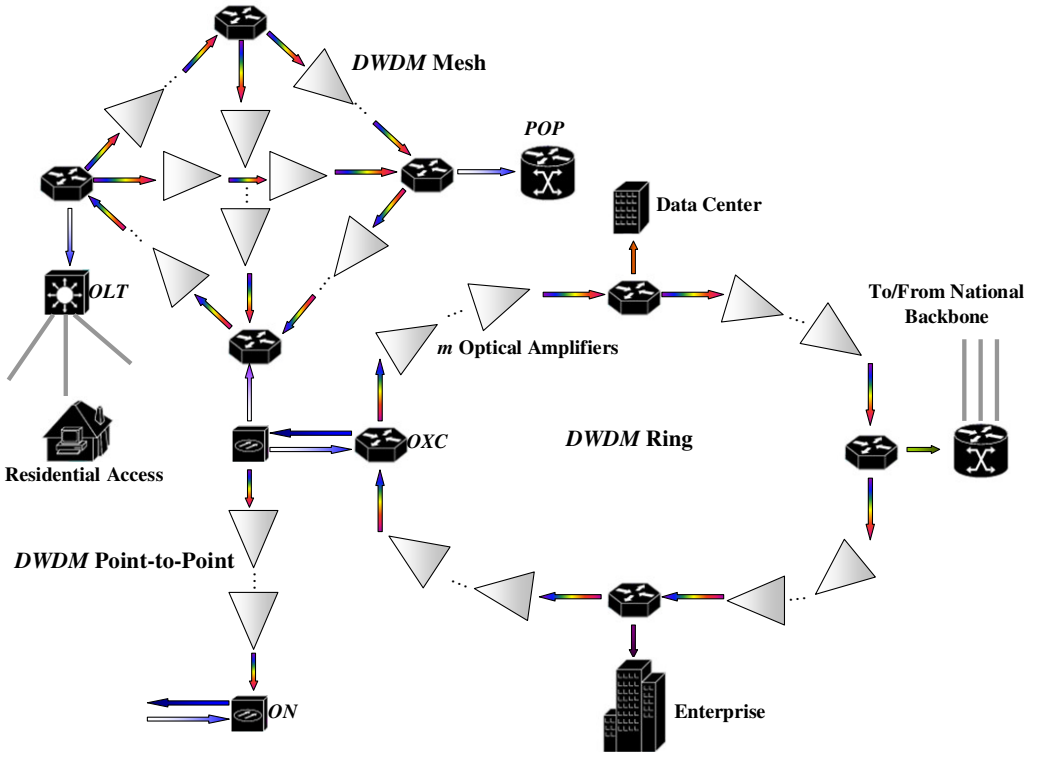

Figure 1-1 *DWDM* optical network: Optical Line Terminal (*OLT*), Optical Cross-Connect (*OXC*), Optical Node (*ON*), Point of Presence (*POP*).

Next-generation *DWDM* systems provide the ability to remotely configure (under software control) which wavelengths are added/dropped, or passing through a node. These systems are classified as re-configurable optical add/drop multiplexers (*ROADM*s) (

Figure 1-2).

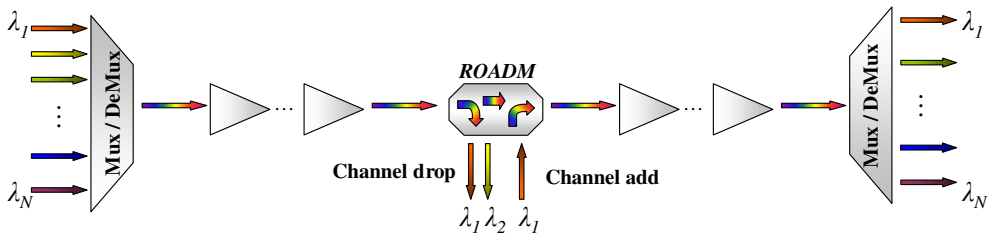

Figure 1-2 *DWDM* link with a re-configurable optical add/drop multiplexer (*ROADM*).

Figure 1-2 illustrates the *ROADM* concept, where *N* channels are multiplexed into a *DWDM* signal propagating over a single fiber. On the *ROADM* channels 1 and 2 are dropped and channel 1 is added again. After the *ROADM* the *DWDM* signal

propagates along the link until the demultiplexer with one less channel. Concerning clients' variable bandwidth needs at different time at different nodes, the amount of channels that are dropped can be remotely reconfigurable.

The enabling of *ROADM* technologies has several tradeoffs. One of the impacts of using *ROADM* is the transient response of the optical amplifiers to traffic re-direction. These abrupt add/drops result in fluctuations in the power of each channel producing significant optical power transients that propagate along the optical amplifiers throughout the network. As an example, when an *EDFA* is at a steady state, it has a determined total output power, which depends on the gain experienced by each channel that in addition depends on the pump power, the fiber length and the emission and absorption cross-sections. Neglecting the *EDFA* internal losses, when channels are dropped or added there is a change in the system initial conditions. The pump power available is going to be distributed by fewer channels after a channel drop or, vice-versa, by more channels after a channel add. Thus, the output power of each channel experience a power transient until it reaches a steady state. Such abrupt power fluctuations are expected to become more commonplace in Wavelength Routed Optical Networks (*WRON*s) and in future optical packet switched networks.

Causes of transients may be classified mainly in two groups. The first one, "predictable", caused by upgrades or downgrades, traffic re-directioning or dynamic changes in cross-connects, includes in general causes that may be controlled in the commissioning and planning of a network. Examples of these scenarios are Figure 1-2 and Figure 1-3.

Figure 1-2 represents a point-to-point link with a *ROADM* in the middle. Due to changes on traffic demands, upgrades and downgrades on the optical link may be needed. Thus, after a new configuration of the *ROADM* a power transient on the remaining channels occurs and is possible to use planning techniques to reduce its impacts, since the *"worst case scenario"* is already known. Another example is the one presented on Figure 1-3 that exposes a *WRON* with the ability of remotely reconfigurable *OXC*. The letters in Figure 1-3 illustrate several points of the network. B and E represents two *OXC* of the network and the remaining letters (A, C, D, F, G,

H) possible propagation directions. The optical link established between A and G by λ_1 is highlighted (continuous red arrow) and the system is at steady state.

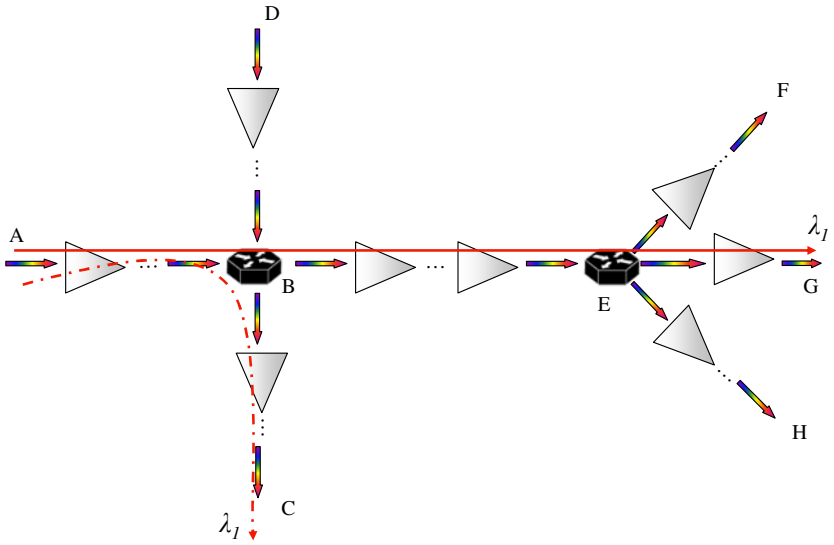

Figure 1-3 *DWDM* network with a re-configurable *OXC*.

A sudden growth on the traffic demand at point C leads to an increase of the available bandwidth needs. Thus, to face this novel scenario the *OXC* at point B is configured to deploy an optical link between A and C using channel λ_1 (dashed red arrow). This sudden change on λ_1 path leads to a power a transient on the remaining channels of the *DWDM* signals propagating along the network. The path BEF, BEG and BEH will experience a power transient due to λ_1 drop and path BC will experience a power transient on remaining channels due to λ_1 addition.

The second type of transients defined as “unpredictable” are caused by fiber cuts, which result from sporadic unexpected events. The response to these types of transients has to be included in the planning of the optical link or with transient control mechanisms. Figure 1-4 illustrates the same network of Figure 1-3 with three groups of *DWDM* signals (yellow, red, blue). The system is at steady state when a fiber cut occurs on path AB, leading to a total disappearance (drop) of the red group of channels. A power transient due to a drop is going to be experienced by the yellow group of channels on the path BEG.

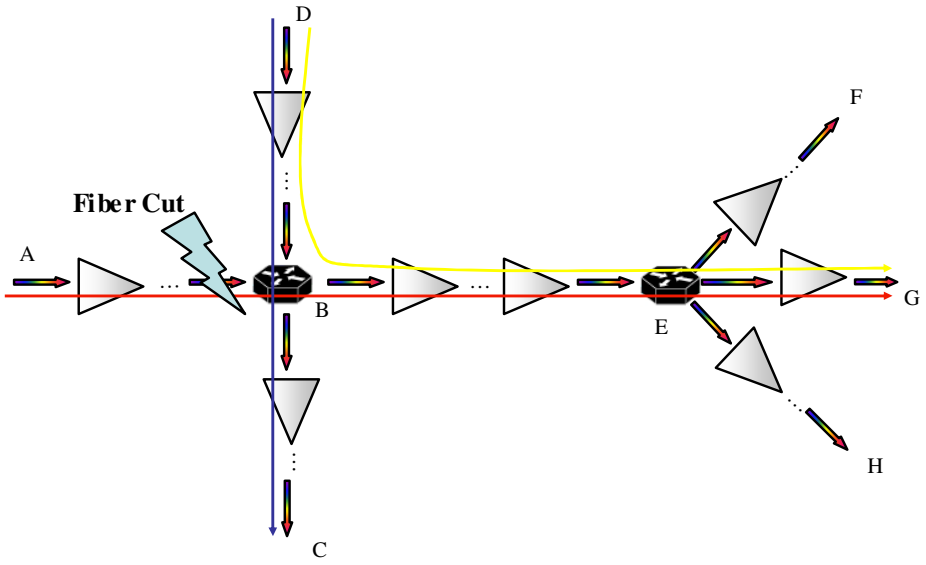

Figure 1-4 Fiber cut on a *DWDM* network.

Previous studies [8], [9] have shown that fast power fluctuations result in optical performance degradation [10], [11]. The *EDFA* transient response has been studied both experimentally and theoretically, and several analytical models have been developed [11], [12]-[19]. The important parameters which characterize the transient phenomenon are the level of power excursion, settling time measured as the time in which the transient decays down to certain value, overshoot and undershoot (described on section 2.2) [14]. Although these power transients will generally be slow in a single amplifier, the speed accumulates from stage to stage and for large number of *EDFA*s, the power transients can be very fast, beyond the ability of automatic gain control circuit of the optical receiver [16]. In order to avoid performance degradation of the optical network, an amplifier must be able to adjust its gain as the number of channels change. Channel populations can change rapidly in failure scenarios such as fiber cuts and, therefore, the transient performance for the amplifier's gain control is critical. (Described in section 2.5).

1.3 Structure and Objectives

The first goal of this project is the implementation a dynamic model of an *EDFA*. A second goal is the comprehension of the transient response. The previously described

model is then used to simulate transient in optical networks links, in order to have theoretical understanding of the problem and also the impact on the network performance. The third goal is to accomplish several experiments to validate the analytical simulations.

The report is organized in 5 chapters. In the interest of brevity, the chapters present the most important results. Forward is a description of the content of each chapter individually.

Chapter 2 has as main objectives to introduce the general concepts of transients, illustrate the parameters used in this work to characterize a transient, present and validate the analytic model. The chapter starts with an overall description of the general concepts used on *EDFA* power transients. Follows a presentation of the standard parameters used in this work to characterize the power transients. Special attention is given to state of the art on power transients and to previous results obtained. In this chapter the analytical model used is presented and validated by reproducing the results obtained in the work of Bononi *et al.* [11].

Chapter 3 has as main goals to expose power transients' characteristics through several simulations using the defined parameters in chapter 2 and evaluate the impact of transients in optical link. Chapter 3 starts with simulations for optical links with two channels. At first is simulated and analysed a similar scenario to the one presented in the work of Bononi *et al.* [11]. The second simulation aims to understand the transient dependency with the power per channel. Followed simulations using a *DWDM* signal, where the power transient spectral dependency is evaluated. The dependency with number of channels dropped/added is also analysed. The impact of a power transient on a 10 Gbit/s *NRZ* channel is included on the end of this chapter.

In order to validate the results obtained through numerical simulation, several experiences were conducted. The inclusion of these results is presented in chapter 4. The first experience is performed in a two-channel *WDM* scenario where the defined parameters in chapter 2 are used to characterize the power transient. The spectral dependency of a power transient is also analyzed in this experience. The second experience consists in using a twelve-channel *WDM* signal to perform an analysis on

the power transient dependency with the number of channels dropped and also the spectral dependency.

Finally in chapter 5 the main conclusions of this work are summarized and several suggestions for future work are presented.

1.4 Novel contributions

The work reported in this thesis aimed to study the power transients in *DWDM* optical networks. The main contributions of this work are listed in the following.

1. Introduction of simplified second order parameters to characterize a power transient.
2. Definition of acceptable limits for the second order parameters.
3. Study of the power transient response in a chain of amplifiers by simulation.
4. Experimental qualitative validation of the behaviours observed by simulation.

Chapter 2. General Concepts

2.1 Introduction

In this chapter the general concepts of power transients are introduced. Criteria for analysing transients are proposed. A survey on power transient's studies by several authors is presented. Limits, according to the impacts analysis, for the defined criteria's are established. The theoretical dynamic *EDFA* model used in this work is presented and validated. The chapter starts at section 2.2 with an introduction to the intrinsic characteristics of an *EDFA* that lead to power transients, ending with a definition for power transients. In section 2.3 the parameters used to characterize a power transient are presented and a survey of previous transients' studies is presented. The impact of a power transient on the performance of an optical link is presented in section 2.4, through a survey of previous studies. The basic concepts of *BER*, *OSNR* and the *Q*-factor are introduced. The analytical model for performance analysis of an optical link is presented with the assumption of an instantaneous response of the optical receiver. Follows section 2.5, where transients limitations are exposed and network planning requirements are defined. In section 2.6 is presented the analytic dynamic model used to simulate power transients. The section ends with the validation of the model through the replication of Bononi *et al.* [11] results. Finally section 2.7 highlights the conclusions obtained for the previous exposed topics.

2.2 Transient in Optical Amplifiers

The ever-changing traffic demands lead to the dynamic nature of reconfigurable optical networks and hence to the dynamic add and drop of channels. In optical networks using optical amplifiers, such as *EDFA*s and Raman amplifiers, sudden changes in the number of channels change the total optical power in the different links

of the network. Hence, a varying optical power is at the input of the amplifiers, which must follow these power changes. The gain experienced by each channel will depend on the total number of channels passing through the amplifier (Figure 2-1). A sudden change in the number of channels leads to fast gain fluctuations at different wavelengths. It is possible to reference the transient response of an amplifier as a gain fluctuation or a power fluctuation, since both are correlated.

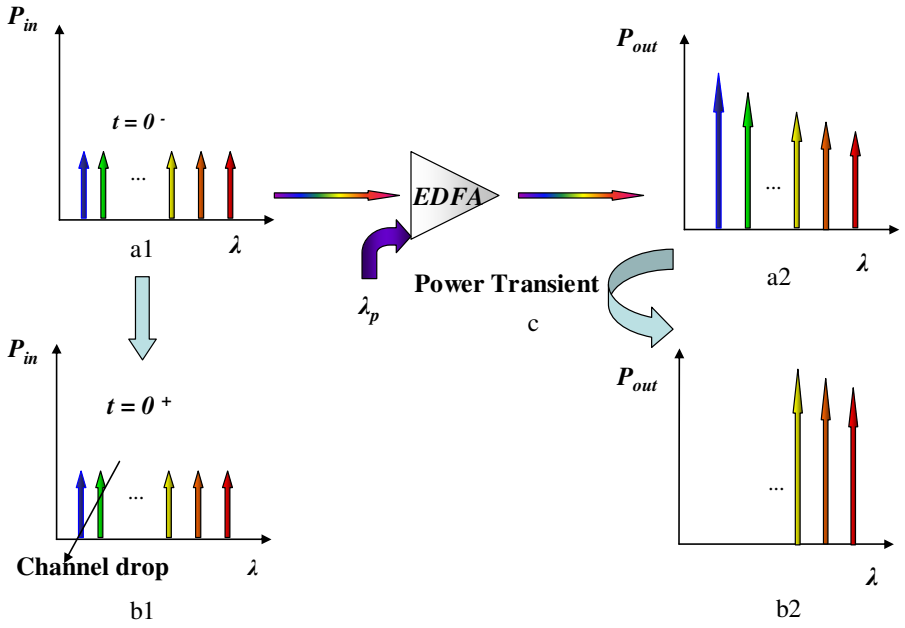

Figure 2-1 Example of an *EDFA* output power variation, in steady-state, after a channel drop.

Figure 2-1 illustrates the behaviour of an *EDFA* when a channel drop occurs. The *EDFA* has *N* channels in the input side with a certain input power per channel, a1. The output power dependency with wavelength, at steady state, is illustrated at a2. At instant $t = 0^+$ two channels are dropped, b1. The output powers of the surviving channels increases, since there is more pump power available. Illustration b2 exhibits the *EDFA* output power per channel, at steady state, after a two-channel drop. The period c, between a2 and b2, is defined as power transient. Thus, a power transient can be defined, as a temporal response of the output power of an *EDFA* to changes in the input power, until the system reaches is novel steady state.

Optical amplifiers may be equipped with several control mechanisms, such as: gain control, output power control or current control. In this work, the transient response will be analysed in optical networks assuming *EDFA*s with pump current control

which is set to constant pump power, since it is the simplest *EDFA* control mechanism. With this type of control mechanism, the transient response of an *EDFA* will depend mainly on its physical characteristics. As such, the presented results may be applied to the design of additional control mechanisms such as gain or output power control.

2.3 Parameters to Characterize Transients in Optical Links

To better understand the transient phenomenon it is important to define how to characterize the transient response.

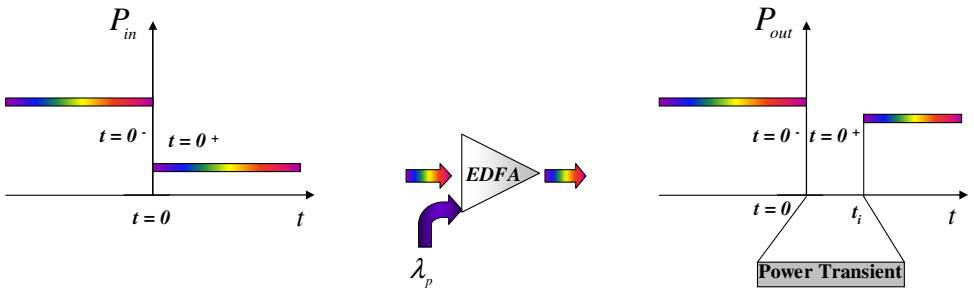

Figure 2-2 Output power variation of an *EDFA* in time domain after a channel drop (steady-state).

Figure 2-2 represents a power transient in a single *EDFA* after a channel drop. The figure exhibits three different illustrations: (a), (b), and (c). Illustration (a) represents the total input power (P_{in}) over time. Instant $t=0$ represents the point in time when a channel drop occurs. At $t=0^+$ the P_{in} has lower value than at $t=0^-$ due to the channel drop. Thus, at $t=0$ a fast power fluctuation (power step) occurs at the input of the *EDFA*, represented on illustration (b). This power step leads to a variation in time of the total output power, which is illustrated through (c). What happens in the time interval between $t=0$ and t_i, the period considered for the transient event (which the criteria will be defined afterwards), is the focus of this work (represented in grey on illustration (c)).

To characterize the transient response, several amplifier characteristics can be analysed: channel output power, gain, power excursion and total output power. Output power, $P_{out}(t)$, represents the power transient response in a specific surviving channel. The gain characteristic represents the transient gain response of a specific surviving

channel over time and is given by: $G(t) = P_{out}(t)/P_{in}(t)$. Figure 2-3 and Figure 2-4 illustrate the four main characteristics used to describe the transient response within the grey period illustrated on Figure 2-2 (c). Figure 2-3 a) illustrates the P_{out} characteristic after a channels drop in a single *EDFA*. Figure 2-3 b) illustrates the gain characteristic.

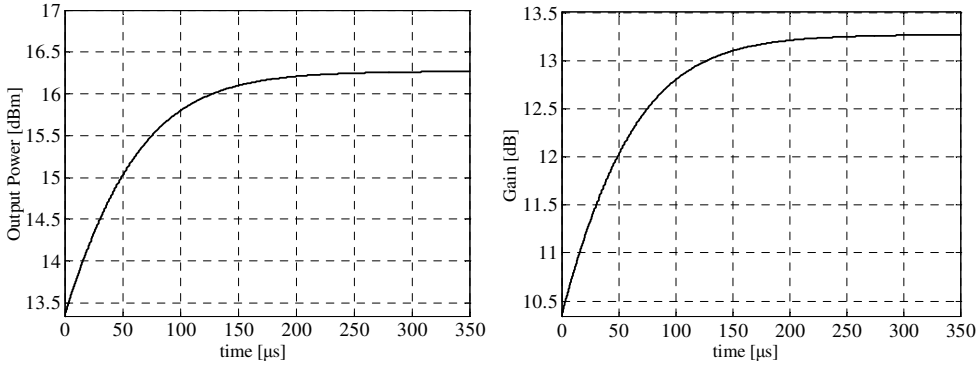

Figure 2-3 Transient response after a channel drop in a single *EDFA*, (a) Output Power (P_{out}) , (b) Gain (G).

The power excursion (Pe) is defined as $Pe(t) = P_{out}(t, t > t_0) / P_{out}(t_0^-)$. Total output power characteristic is a time representation of the transient response of the sum of the output power of each channel, P_{out}^{total}.

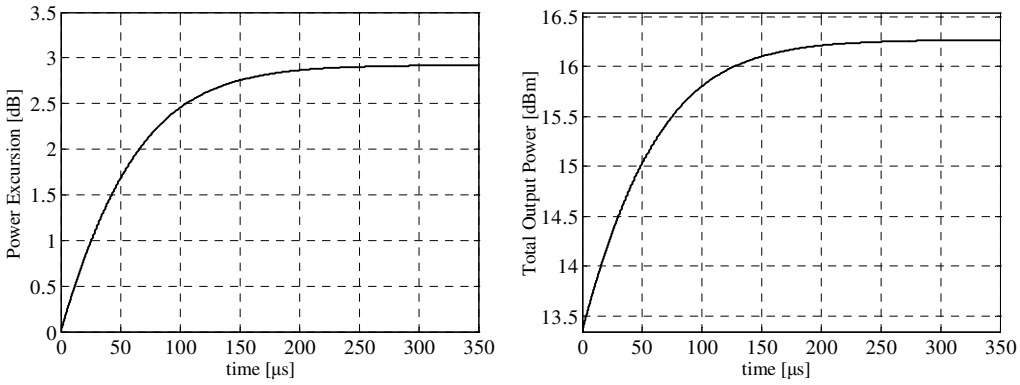

Figure 2-4 Transient response after a channel drop in a single *EDFA*, (a) Power excursion (Pe) , (b) Total output power (P_{out}^{total}).

Figure 2-4 a) illustrates Pe characteristic to a channel drop in a single *EDFA* and Figure 2-4 b) exhibits the P_{out}^{total} characteristic. In this work, special attention is given to the P_{out} and Pe characteristic. Follows the presentation of the parameters used to describe a transient response focused on P_{out} and Pe characteristic.

In a chain of amplifiers the power transient has an oscillatory response, which can be described with time domain specifications typically used to analyse control systems

[20]. The considered response parameters may be: rise time/fall time (*tr*), settling time (*t*s), overshoot (*Mp*), undershoot (*mp*) and peak time (*tp*).

The rise/fall time is the time the system takes to reach the vicinity (90%) of its new set point. Settling time is the time the system transient takes to decay within a given margin of the set point. In this work, this margin will be assumed as 2% of the set point. The overshoot is ratio between the system steady-state, considered at settling time and the system peak value. This is analogous for undershoot specification. The peak time is the time the system takes to reach the maximum (minimum in an add channel situation) value. Figure 2-5 illustrates these specifications on $P_{out.}$

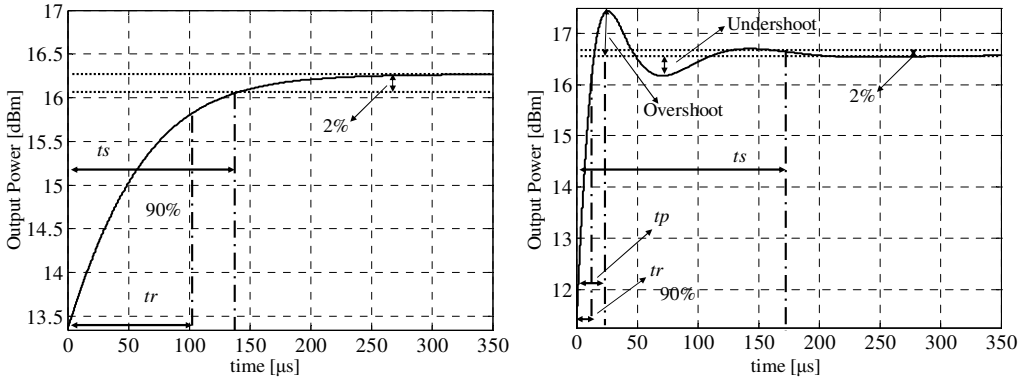

Figure 2-5 Transient output power response of a channel drop in: a) 1 *EDFA*; b) a chain of 10 *EDFA*s.

The time domain parameters are analyzed through the P_{out} characteristic. These parameters are used to evaluate the power excursion characteristic at these specific instants: Pe_{tr}, Pe_{tp}, Pe_{ts} and Pe_{mp}. It is important to evaluate the power excursion within the grey period illustrated on Figure 2-2 (c) and also obtain the slew rate imposed by a transient. The slew rate, *SR*, may be obtained from the ratio Pe_{tr}/tr.

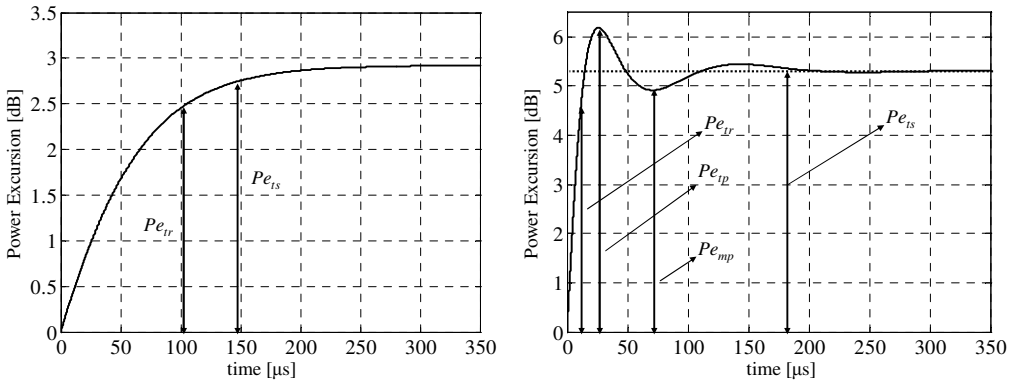

Figure 2-6 Transient power excursion of a channel drop: in 1 *EDFA*; b) in a chain of 10 *EDFA*s.

Several studies have been presented to describe and understand the transient behaviour on *EDFA*s. A study by Y. Sun *et al.* in [18] has presented a simple model for characterising the dynamic behaviour of an *EDFA* when there are changes on the total number of channels at the *EDFA* input. The time dependent gain is described by a single ordinary differential equation for an *EDFA* with arbitrary number of channels, power levels and propagation directions. This model agrees with experimental results, such as the work by A. Srivastava *et al.* in [19]. Y. Sun *et al.* also presented an experimental work where power transients have been analysed in a chain of *EDFA*s [21]. The authors have reported on total output power transients of 1 dB in less than 3 μs in a chain of five *EDFA*s. These fast power variations result from the collective behaviour of the amplifier chain. A. Bononi *et al.* have conducted a theoretical study in *EDFA* dynamics where the transient response in an amplifier chain is greatly exposed [11]. The authors have reported that the transient response when channels are added reaches a steady state condition faster than when channels are dropped. This results from the fact that *EDFA* dynamics are connected to the depletion and the refill of the reservoir, which was the term used by the authors to designate the total number of excited ions. While the refill process is mainly contributed by the pump, and is a process in which one pump photon can excite at most one ion, the depletion process is mainly caused by signals, and is an avalanche process connected to stimulated emission: one signal input photon can stimulate a very large number of excited ions in the reservoir. Thus, the time scales connected to the depletion process can be extremely fast, while those connected to the refill process are slow and depend on the pump power and the total number of dopant ions. In any case, the amplifier dynamics are essentially independent of the fluorescence time, which is the decay time of an excited ion. As a consequence, channel addition causes much faster transients than channel dropping. In a scenario with only two channels, when one is dropped, the peak time decreases with the number of amplifiers in the chain. After 20 *EDFA*s is less than 25 μs and the power excursion on the surviving channel can go up to 10 dB.

2.4 Impact of Power Transients on the Performance of an Optical Link

Previous studies have shown that fast power changes might result in *OSNR* changes. Fast power changes may trigger non-linear effects in fiber propagation resulting in significant *BER*. *OSNR* changes leads to *Q* – factor variations. The work by M. Hayee *et al.*, described in [8] has presented an analysis of fiber transmission penalties due to nonlinearity and *ASE* noise resulting from channel drop-add *EDFA* gain and power transients in a chain of 10-20 *EDFA*s with as many as 32 channels. There is no correspondence between this analysis and the previously defined parameters for the power transient response (section 2.2) but provides insight on the impact of transients. The authors have reported that transient penalties depend upon the data rate, number of channels and fiber type. Hence, given *N*-1 dropped channels in an *N* channel system, they found that the output power transient increases due to channel dropping severely degrades the performance of the surviving channel because of self-phase modulation (*SPM*). In a 16-channel system, after 15 channels are dropped, the *Q*-factor of the surviving channel decreases 30 dB in a cascade of 20 *EDFA*s, for a period of less than 100 μs due to the degrading effect of *SPM*. This penalty is more severe in single mode fibers (*SMF*) than in dispersion-shifted fibers (*DSF*). In addition the *OSNR* increases approximately 8 dB because the power of the surviving channels increases. However, this power per channel increase may trigger a non-linear effect which leads to a decrease of the *Q*-factor. Channel adding degrades all channels due to cross-phase modulation (*XPM*) and four wave mixing (*FWM*). The *Q*-factor of the remaining channel decreases approximately 8dB in less than 100 μs.

In this work the system *OSNR* after the first *EDFA* is defined by the following equation, assuming that the noise power has the same time behaviour of the gain, [22]:

$$OSNR(t) = \frac{P_{out}(t)}{NF\, G(t)\, h\, f\, \Delta f}, \qquad (2.1)$$

NF is a typical noise figure used in network dimension, G the instantaneous gain, h Planck's constant, f the optical signal frequency, Δf, is a reference bandwidth for the noise measurement, typically 12.5GHz (≈0.1 nm).

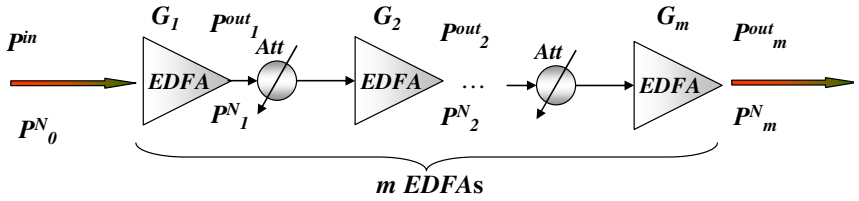

Figure 2-7 Simplified noise model in a chain of *EDFA*S.

Figure 2-7 illustrates a chain of *m EDFA*s where P^N_m represents the noise power at the output of the m^{th} EDFA,

$$P_m^N(t) = P_{m-1}^N(t) G_m(t) Att + NFhG_m(t)\Delta f \ . \tag{2.2}$$

The time behaviour of $OSNR(t)$ after the m^{th} *EDFA* is given by $P_m^{out}(t)/P_m^N(t)$. The *OSNR* excursion can be defined as $OSNRe(t) = OSNR_{out}(t > t_0)/OSNR_{out}(t_0^-)$.

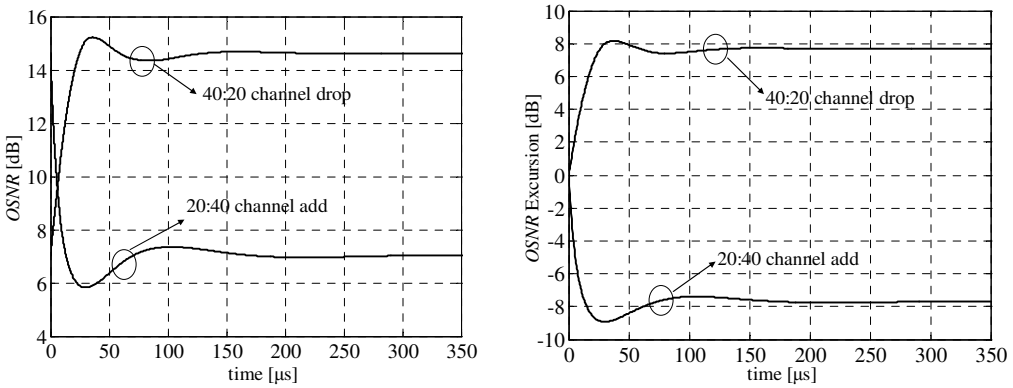

Figure 2-8 Transient response after 20 channels are dropped/added in 40 channel *DWDM* signal in a chain of 10 *EDFA*s a) *OSNR* time behaviour b) *OSNR* Excursion time behaviour.

Figure 2-8 a) illustrates the *OSNR* transient response of a specific channel when channels are dropped and added. The *OSNR* exhibits an oscillatory response and it is possible to observe that the *OSNR* increases when channels are dropped and decreases when channels are added. A channel drop leads to an increase of the *OSNR* ratio since the power available for a surviving channel increases. A channel add leads to a decrease of the *OSNR*, the power available per channel reduces leading to an *OSNR*

decrease. Figure 2-8 b) exhibits the *OSNR* excursion characteristic which allows a good understanding of the transient impact on the *OSNR* characteristic.

The system performance parameter *Q*-factor is described as below, using the system *OSNR* [22]:

$$Q(t) = \frac{2\,OSNR(t)\,\Delta f / B_o}{1+\sqrt{1+4\,OSNR(t)\,\Delta f / B_o}}\sqrt{\frac{B_o}{B_e}}. \qquad (2.3)$$

Equation (2.3) has under consideration an infinite extinction ratio and no inter-symbolic interference. B_e and B_o are the bandwidths at cut-off -3dB frequency of the electrical and the optical filters, respectively, used in a reference optical receiver. Assuming for simplicity that $B_0 \approx 4B_e$, for 10Gb/s signals. Thus the bandwidth of the optical filter is considered wide enough to only consider *ASE* as a noise source. Figure 2-9 illustrates a simplified representation of an optical receiver, with a *PIN* photo detector followed by an automatic gain control (*AGC*) system.

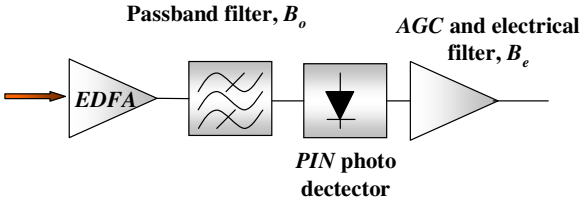

Figure 2-9 Simplified diagram for the considered optical receiver.

From (2.3) it is possible to obtain Figure 2-10 a), which exhibits the *Q*-factor time behaviour with the drop and addition of channels. Figure 2-10 b) exhibits the *Q*-factor excursion, which is defined as $Qe(t) = Q_{out}(t, t > t_0) \big/ Q_{out}(t_0^-)$.

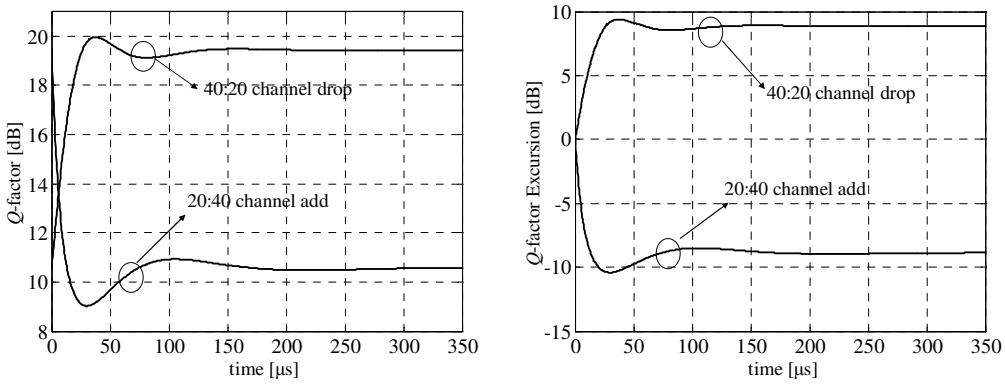

Figure 2-10 Transient response after 20 channels are dropped/added in 40 channel *DWDM* signal in a chain of 10 *EDFA*s a) *Q*-factor time behaviour $B_o = 4B_e$; B_e = 10GHz b) *Q*-factor Excursion time behaviour.

The *Q*-factor excursion is another characteristic of interest in this work since exposes the impact of a power transient in the system performance. Therefore, the previously defined parameters used to characterize P_{out} and *Pe* are now applied to *OSNRe* and *Qe*.

Figure 2-11 a) illustrates the parameters applied to the *OSNRe* characteristic after a channel drop. Analogous to power excursion chart, the *OSNR* excursion can be analyzed at these instants: $OSNRe_{tr}$, $OSNRe_{tp}$, $OSNRe_{mp}$ and $OSNRe_{ts}$.

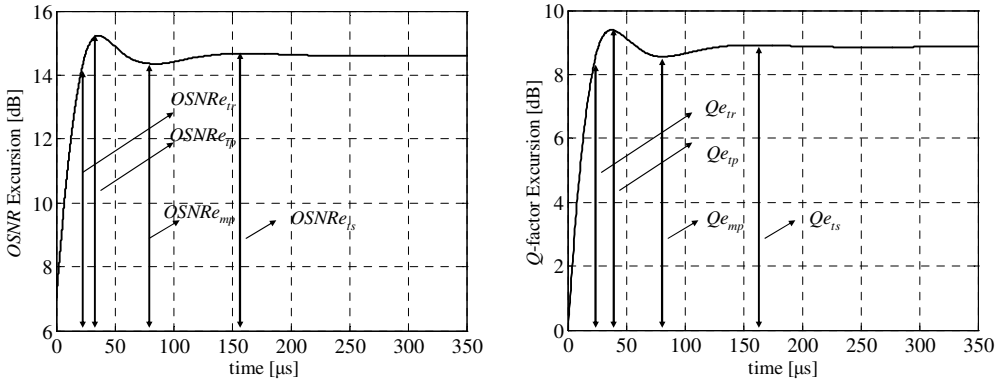

Figure 2-11 Time domain parameters applied to a) *OSNR* Excursion b) *Q-factor* Excursion.

Figure 2-11 b) exhibits the defined parameters applied to *Qe* characteristic of a channel drop. Regarding the *Q*-factor excursion characteristic the focus of this work is also the value associated at the parameter instant, this is: Qe_{tr}, Qe_{tp}, Qe_{mp} and Qe_{ts}.

The *Q*- factor is related with *BER* through [3]:

$$BER(t) = \frac{1}{2} erfc\left(\frac{Q(t)}{\sqrt{2}}\right) \tag{2.4}$$

where $erfc(u)$ is the complementary error function given by $erfc(u) = 2/\sqrt{\pi} . \int_u^{\infty} e^{-\lambda^2} d\lambda$. Note that the time variant *BER* is in fact an abstract entity, since it is not possible to define an instantaneous *BER.* Instead, one may consider that this is a time-resolved *BER* that could be measured by taking multiple measurements at instant *t*, from the resulting average extract the *BER*. This technique is used by W. Wong *et al.* in a study described in [23] and is the same method used in this study. In this work, the time resolved *BER* may be approximated, for binary intensity modulated *NRZ* signals using direct detection, according to (2.4).

Figure 2-12 illustrates the time behaviour of *BER* in a channel after twenty channels are added.

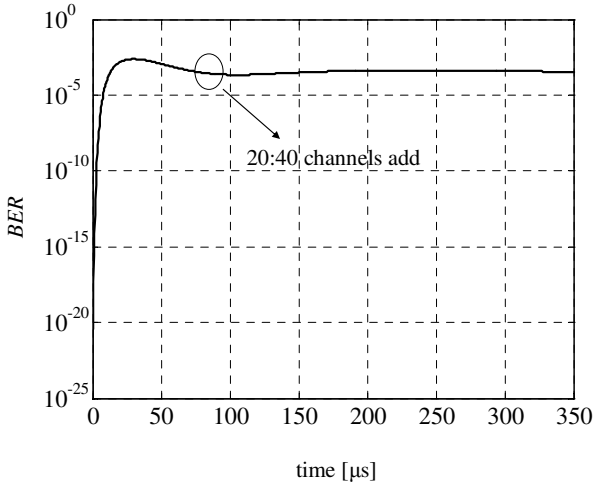

Figure 2-12 *BER* time behaviour when 20 channels are added, B_o = 40GHz and B_e = 10GHz.

2.5 Limitations due to transients and requirements

Previously was presented a simplified set of transient parameters, which may be used to characterize the temporal response of an *EDFA* due to its similarity to a second order linear-invariant system response to power and noise fluctuations at its input. At this point is important to present the application of these parameters to the definition of engineering rules for the design of optical networks resilient to transients. The

imposed limits are the typical requirements used in *DWDM* network planning commercial available.

2.5.1 Limitation due to fiber nonlinearities

The over-increase of power per channel may lead to substantial degradation due to fiber nonlinearities, hence it must be considered here. Generally, one may assume that the network is planned to support the impact of fiber nonlinearities in the case of static operation. However, degradation may arise in case of transients when the power per channel injected in the fiber overshoots above the limits defined by the initial planning. This may lead to degradation due to *SPM*, *XPM* and *FWM*. Such overshoots may occur in the case of channel drops or fiber breaks, when the number of channels at the input of an *EDFA* is suddenly reduced. When this occurs, the *EDFA* may over-amplify the surviving channels, increasing their power to higher static level. One may assume that, the network is prepared to support the higher static level. Therefore, it is necessary to ensure that the power overshoot of each channel due to the transient does not exceed significantly the static power level after the transient. In this work, it will be assumed that the maximum excess of any given channel due to transients is 1 dB above the static power level after the transient. This leads to a maximum power per channel overshoot of approximately 26% for channel drops or fiber breaks.

Note that the fiber nonlinearities may also be used to define a maximum absolute power per channel. A simple estimate of this power level has been conducted by Elbers *et al.* in [24], providing limitations regarding *SPM*. However, this type of analysis will not be followed in this work.

2.5.2 Limitation due to *OSNR* fluctuations

Opposite to the limitation due to fiber nonlinearities, the over-decrease of power per channel may lead to prohibitive levels of *OSNR*, generating error bursts. Substantial *OSNR* reduction may occur when channels are added to the *WDM* signal at an *EDFA* input, leading to the reduction of the output power of all the channels at the *EDFA* output. Once again, one may assume that the network is prepared to handle the static levels of *OSNR* that are presented before and after any possible transient. However, the transient planning must ensure that the minimum *OSNR* during a transient is

within a given margin of a static level after a transient. Taking the same assumption as previously for fiber nonlinearities, it will be considered here that the minimum *OSNR* excursion during a transient should be below 1 dB of the static *OSNR* level after the transient.

2.5.3 Limitations of the receiver response

The main limitations of the optical receiver response are related to the dynamic power range between the receiver sensitivity (minimum power limit) and the receiver overload (maximum power limit), and the temporal response of the *AGC* system that usually follows the photo detector. In all cases, these limitations depend on the specific characteristics of the photo detector and following circuitry, and vary significantly from manufacturer to manufacturer. Table 1 presents a set of typical power values for sensitivity at a *BER* of 10^{-12} and overload, extracted from [4]. From this set of values, it is easy to conclude that for a typical optical receiver for 10 Gb/s signals using an *EDFA* as optical pre-amplifier followed by an optical filter with a typical insertion loss of 5 dB, a *PIN* photo detector and corresponding *AGC* circuitry, as illustrated in Figure 2-9, would tolerate absolute power fluctuations at the *EDFA* output between -13dBm and 4dBm. This example will be used along this work as a reference.

Bit Rate	Type	Sensitivity	Overload Parameter
155 Mb/s	*pinFET*	-36 dBm	-7 dBm
622 Mb/s	*pinFET*	-32 dBm	-7 dBm
2.5 Gb/s	*pinFET*	-23 dBm	-3 dBm
2.5 Gb/s	*APD*	-34 dBm	-8 dBm
10 Gb/s	*pinFET*	-18 dBm	-1 dBm
10 Gb/s	*APD*	-24 dBm	-6 dBm
40 Gb/s	*pinFET*	-7 dBm	3 dBm

Table 1 Typical sensitivities of different types of receivers without optical pre-amplification in the 1.55 µm wavelength band measured at the *BER* of 10^{-12} using a pseudo-random 2^{23} -1 sequence.

Perhaps more difficult to define is the response of the *AGC*. In fact, if the transient response of the amplifier is slow, the *AGC* should have no difficulty in maintaining a

constant output level. However, as the transient response becomes faster, the *AGC* may no longer be able to follow the power change appropriately, hence giving rise to error burst.

A simple way to characterize the *AGC* response is using the maximum slew rate. In this work, it will be considered that the maximum response of an *AGC* for a 10 Gb/s receiver is typically 0.5 dB/μs, which is relatively slow but can be used to gain insight on the limitations imposed by transients in an optical network.

In summary, the limitations for the *EDFA* transients defined in this work are as follows:

1. Maximum of 26% of overshoot in case of channel drop or fiber break due to fiber nonlinearities.
2. Maximum of 26% of undershoot in case of channel add to avoid excessive BER.
3. Maximum $OSNRe_{tp}$ of 3 dB to ensure minimum *BER* for *FEC* operation.
4. Maximum difference between $OSNRe_{tp}$ and $OSNRe_{ts}$ of 1dB to ensure minimum *BER* fluctuations.
5. Output power per channel range between -13 dBm and 4 dBm, to ensure operation with power levels above the sensitivity and bellow the overload thresholds.
6. Maximum transient slew rate of 0.5 dB/μs, to ensure effective response of the *AGC* in the optical receiver.

2.6 Erbium-Doped Fiber Amplifiers Dynamic Model

This section describes the basic formalism used for modelling light amplification in *EDFA*s. The *EDFA* model used in this work is a two-level energy model. According to Bononi *et al.* work, described in [11], the dynamic behaviour of an *EDFA* can be described by the dynamic time behaviour of the system's state this is the reservoir $r(t)$. The reservoir represents the total number of excited ions in the amplifier and is a number between "0" and $r_M = \rho A_{eff} L$, which represents the total number of ions in

the doped fiber, where $\rho\left[m^{-3}\right]$ is the ions density, $A_{eff}\left[m^2\right]$ is the effective area of the fiber core and $L[m]$ the amplifier length.

The dynamic behaviour of the reservoir is described by a first-order ordinary differential equation (*ODE*).

$$\frac{\partial r(t)}{\partial t} = -\frac{r(t)}{\tau} - \sum_{j=1}^{N} Q_j^{in}(t)\left[1-\exp\left\{B_j r(t) - A_j\right\}\right]. \tag{2.5}$$

Equation state (2.5) represents the number of available ions ready to be converted into signal photons, where $\tau[s]$ is the fluorescence time and Q^{in} the photon flux per channel at the input of the EDFA. The photon flux, Q $[photons/s]$, is related to the power in watts by $P = Q(hf)$, $[W]$, where f is frequency in hertz, $[Hz]$, and h is Planck's constant in units of $[J/Hz]$. The parameters A_j and B_j which are independent of τ, are introduced to stress that the gain depends on τ only through r. Follows that $A_j = \rho\Gamma_j\sigma_j^a L$ and $B_j = \Gamma_j\sigma_j^T / A_{eff}$, where Γ_j, $\sigma_j^e\left[m^2\right]$, and $\sigma_j^a\left[m^2\right]$ are the confinement factor, and the emission and absorption cross sections of channel *j*, respectively, and $\sigma_j^T = \sigma_j^e + \sigma_j^a$. The pump is placed on channel 1. The standard parameters used in [15], [18], [19] and [21], are the absorption coefficients $\alpha_j = \rho\Gamma_j\sigma_j^a = A_j/L$ and the intrinsic saturation powers $P_j^{IS} = hfA/\Gamma_j\sigma_j^T\tau = hf/B_j\tau$. The photon flux per channel at the output of the *EDFA* is given by $Q_j^{out}(t) = Q_j^{in}(t)\exp\left[G_j(t)\right]$, where $G_j(t) = B_j r(t) - A_j$, $\quad j = 1,...,N$.

The initial condition $r(0)$ can be any number in the allowed range $[0, r_M]$. If at a time $t = 0^-$, one instant before start of the observation period, the amplifier is at steady state, then $r(0)$ must satisfy (2.5) with $\partial r/\partial t\big|_{t=0^-} = 0$

$$r(0) = \tau\sum_{j=1}^{N} Q_j^{in}\left(0^-\right)\left[1-\exp\left\{B_j r(0) - A_j\right\}\right] \tag{2.6}$$

which is the steady-state equation of the doped amplifier [25].

The direction of propagation of the input fluxes through the *EDFA* has no effect on r. Hence co- and counter propagating pumping are equivalent in this analysis. The *ASE* has been neglected in this analysis, and in fact a co propagating pump always gives a larger *OSNR* [2]. In the following simulations, to solve the *ODE*, a numerical algorithm named Runge-Kutta method is used. The inbuilt Matlab program, named *ODE*45, is used to apply this method.

2.6.1 Add and drop of channels in a single *EDFA*

In a single amplifier, described by (2.5), at time $t = 0^-$ (an instant before time 0), given the initial value $r(0)$ and the input fluxes $\left\{Q_j^{in}\left(0^-\right)\right\}$ [1]. The system is at steady state at $t = 0^-$. At time $t = 0^+$ each input flux undergoes a discontinuity and then remains constant for all $t > 0$. This discontinuity simulates a channel drop or a channel addition, according with

$$Q_j^{in}(t) = Q_j^{in}\left(0^-\right) + \Delta Q_j^{in} \quad j = 1,...,N. \tag{2.7}$$

Consider an example very similar to the ones presented in [11], [13] and [26]. The amplifier has two input channels λ_1 = 1552.4 nm, λ_2 = 1557.9 nm, with initial input powers of -2dBm/Channel and -2 + 10log10(7) dBm, simulating a total of nine channels. The amplifier is pumped at 980 nm, with pump power of 18.4 dBm, and has L = 35 m, τ = 10 ms.

The absorption coefficients are 0.257, 0.145, 0.125 m^{-1} and the intrinsic saturation powers are 0.440, 0.197, 0.214 mW at 980, 1552.4, 1557.9 nm, respectively. The system is at equilibrium before $t = 0$. At time $t = 0$ part of the power on channel 2 is dropped/added simulating a drop of four and seven channels and the addition of seven channels.

[1] Note that $r\left(0^+\right) = r\left(0^-\right)$ since $\partial r/\partial t\big|_{t=0}$ exists.

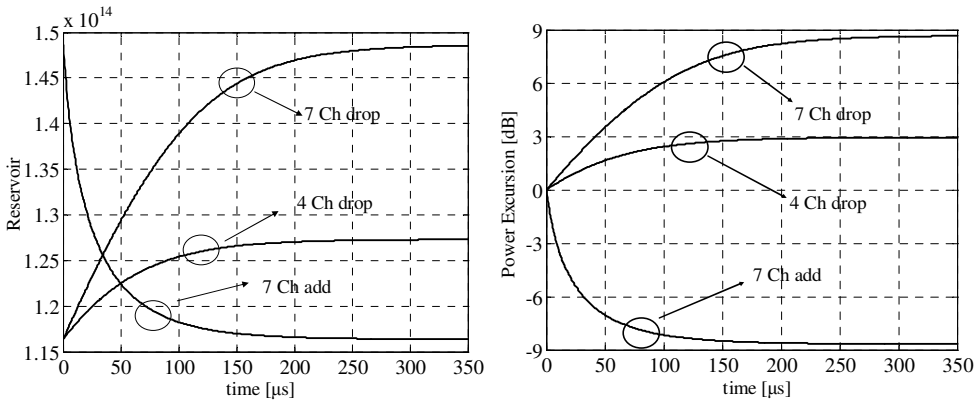

Figure 2-13 Time evolution of the transient response when 7Chs are dropped/added and 4Chs are dropped, with two *CW* signals, -2 dBm/Ch, *L*=35m and a 980 nm Pump of 18.4 dBm: a) reservoir, b) Power Excursion.

Figure 2-13 a) shows the reservoir dynamics for the solution of (2.5). It is possible to observe that the total number of excited ions increases with a channel drop and decreases when channels are added. The drop of seven channels leads to more excited ions available for amplifying the remaining channel than when only four channels are dropped. Figure 2-13 a) demonstrates the result obtained by Bononi *et al.* work in [11] that the timescales connected to the addition of channels process are faster than those connected to the drop of channels.

Figure 2-13 b) shows the corresponding power excursion, *Pe*, on the surviving channel (Ch1). The *Pe* is higher for a seven channel drop than when only four channels are added, because there are more excited ions available. Although the transient response is faster when channels are added, the *Pe* when seven channels are added or dropped converges to the same absolute value. In addition, Figure 2-14 a) illustrates the time evolution of the P_{out} on Ch1 and Figure 2-14 b) exposes the time evolution of the *EDFA* gain for Ch1.

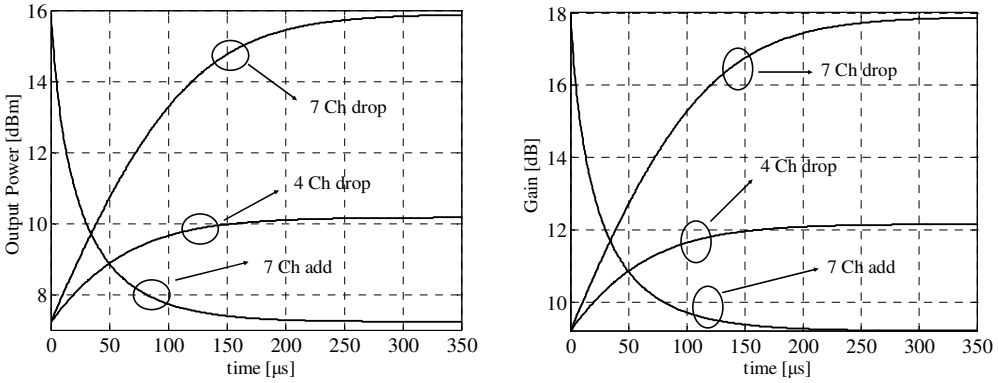

Figure 2-14 Time evolution of the Ch1 after a 7Chs drop, 4Chs drop and 7Chs add with two *CW* signals, -2dBm/Ch, *L*=35m, 980 nm pump of 18.4 dBm: a) Output power, P_{out}, b) Gain, *G*.

In both figures the channel drop simulation has the same start point since the channel under analysis is the same for the two drop simulations. The start point of P_{out} and G is the steady state condition of the system before channels are dropped or added.

2.6.2 Add and drop of channels in an *EDFA* chain

In this section the theory to the study of power transients in a single *EDFA*, exposed on section 2.6.1, is applied to a chain of amplifiers in response to channel dropping/adding, a circuit switching scenario, a case also studied in [11], [26] and [21].

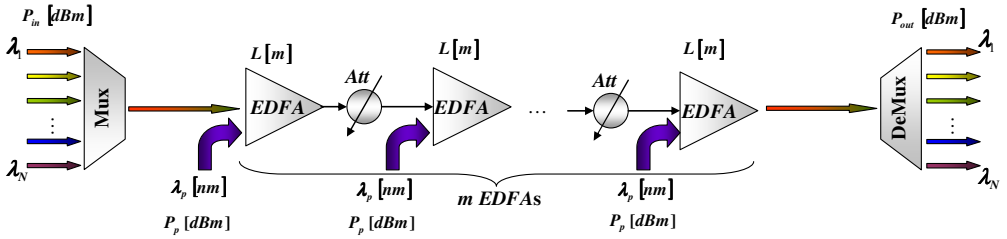

Figure 2-15 Typical *EDFA* chain simulation scneario.

Figure 2-15 illustrates the typical *EDFA* chain scenario used in this work. The chain is composed by *m* identical *EDFA*s. The attenuation is identical between *EDFA*s, the amplified signal is attenuated (*Att*) to simulate the losses imposed by a fiber span. The pump power is injected at the input of every *EDFA*. At time $t = 0^+$ the fluxes at the input of the chain have a discontinuity; such discontinuity propagates along the amplifier chain[1]. Equation (2.5) describes the time variation of reservoir $r_i(t)$ at each

[1] The propagation delay of light in the fiber chain is neglected.

amplifier $i = 1, \cdots, m$ along the chain and (2.6) describes the steady state condition, $r_i(0)$, before the discontinuity at each amplifier. The total power at the input of m^{th} *EDFA* is given by : $P^{in}{}_m(t) = P^{out}{}_{m-1}(t)\,Att$.

As a numerical example, consider an amplifier chain with 20 identical amplifiers (m=20), similar to the one presented in [11].

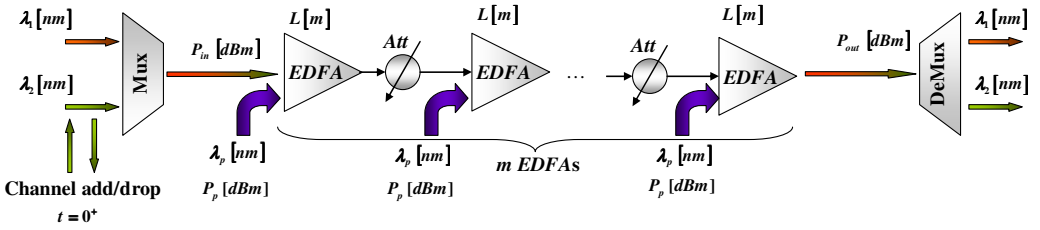

Figure 2-16 Example of a two-channel *WDM* signal in an *m EDFA* chain.

Figure 2-16 illustrates the example used by Bononi *et al.* The amplifier has two input channels λ_1=1552.1 nm and λ_2=1557.7 nm multiplexed into a single fiber, with initial input powers of 3dBm/Channel. The amplifiers (*EDFA*s) are pumped at 980 nm, with a pump power of 18.4 dBm, and have L = 35 m, τ = 10.5 ms. The absorption coefficients are 0.257, 0.145, 0.125 m^{-1} and the intrinsic saturation powers are 0.440, 0.197, 0.124 mW at 980, 1552.1, 1557.7 nm, respectively. The attenuation between each *EDFA* is 10.32 dB. The system is at equilibrium before $t = 0$. At time $t = 0$ the power on channel 2 is dropped/added completely.

Figure 2-17 a) illustrates the time evolution of gain and its dependency with the number of *EDFA*s that compose the amplifier chain. The transient response after the first *EDFA* is identified by m = 1 and after the twentieth *EDFA* by m = 20. The surviving channel acquires a first order gain transient response after the first *EDFA*. As is illustrated, the gain transient after the first *EDFA* has a higher maximum value and achieves its vicinity later than second *EDFA*. With the increasing number of *EDFA*s on the link the gain variations are smaller and faster, acquiring an oscillatory second order response. The input power is variable from *EDFA* to *EDFA* since the attenuation has a fixed value and do not attenuates the exact gain experienced on the previous *EDFA*. *EDFA*s gain depend on the input power, the gain is increases with the

decrease of the input power. Thus, if the input power of the surviving channel increases from *EDFA* to *EDFA* the gain also reduces.

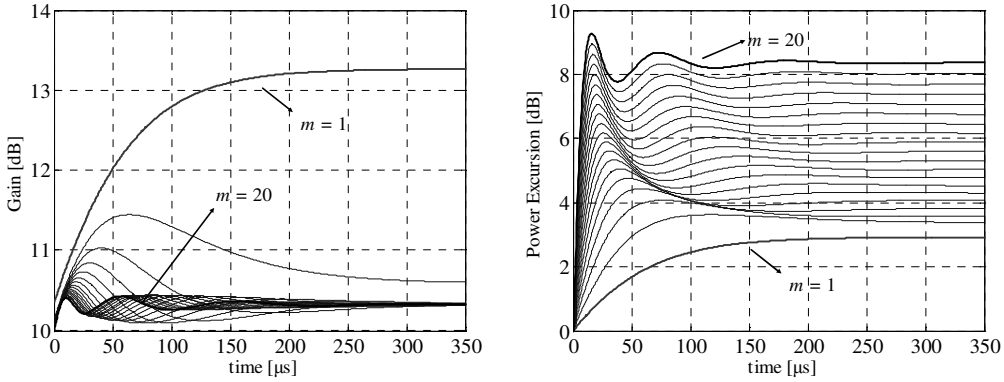

Figure 2-17 Transient response after channel drop from 1 to 20 *EDFA*s a) Gain; b) Power Excursion.

The time behaviour of the input power of each *EDFA* also changes from step behaviour at the input of the first *EDFA* to a first order behaviour at the input of the second *EDFA* and a second order at the input of the third *EDFA*. These input power time variations induce the oscillatory behaviour of the transient (gain and power) response. The power excursion increases (in a drop scenario) from *EDFA* to *EDFA* acquiring an oscillatory behaviour achieving a maximum of approximately 9 dB (Figure 2-17 b)).

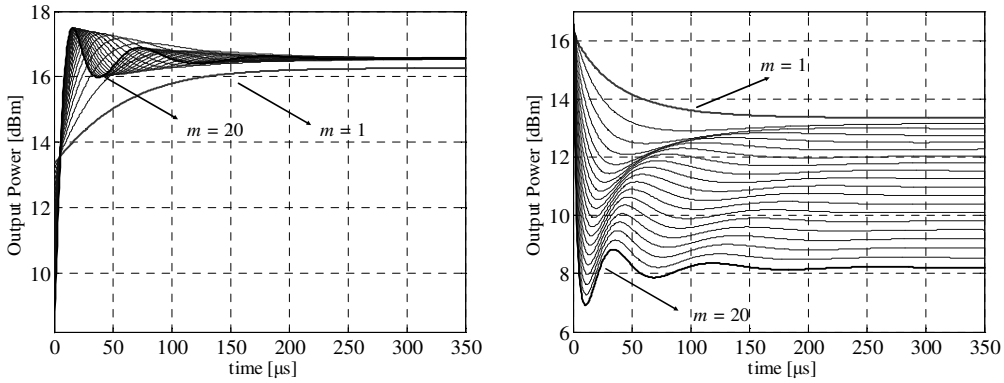

Figure 2-18 Transient response from 1 to 20 *EDFA*s; a) Output power after a channel drop b) Output power after channel add.

Figure 2-18 a) illustrates the output power transient after each *EDFA* on a 20 *EDFA* chain. The output power acquires an oscillatory behaviour after each *EDFA* of the chain. It is possible to observe an increase of the oscillations amplitude from *EDFA* to *EDFA*. Figure 2-18 b) illustrates the power transient behaviour of channel 1 after

channel 2 is added. The output power also acquires an oscillatory with the increase of the *EDFA* number and experience a reduction in absolute power.

This behaviour was expected since with a channel addiction the pump power is distributed, according to the intrinsic *EDFA* characteristics, by the two existing channels.

Figure 2-19 a) exposes the total output power, after channel 2 is added. It is possible to observe that the power after achieving its vicinity has approximately the same absolute value of 16.5 dB that Figure 2-20 a). Figure 2-19 b) exposes the power excursion of channel 1 which achieves, after stabilization, the same absolute value that Figure 2-18 b) of approximately 9 dB.

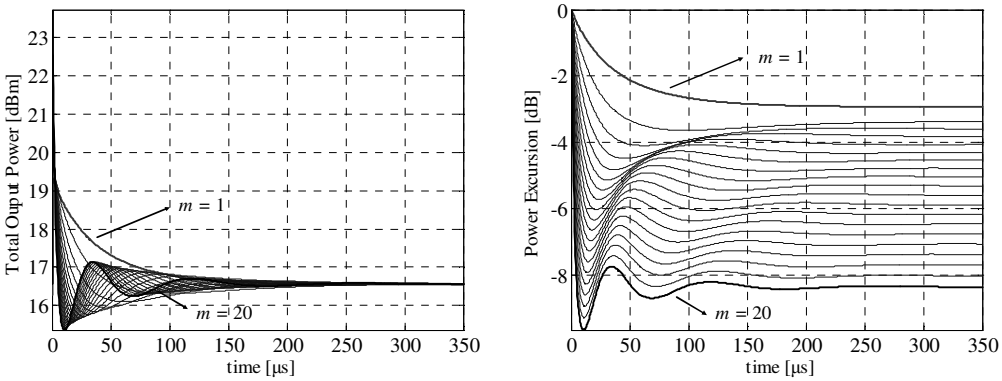

Figure 2-19 Transient response after channel add from 1 to 20 *EDFA*s a) Total output power; b) Power excursion.

These results perfectly match the ones obtained by Bononi *et al.* [11], which validates the analytic model implementation. The presented analytic model has validation limitation due to the fact that is an analytical model for low gain regime, i.e. $G < 20$ dB, where there is no amplifier self-saturation by *ASE.* As a result, both forward and backward *ASE* powers can be ignored and, the *EDFA* can be analyzed as noise-free amplifier, and the effect of gain saturation by high input signals can be taken into account. With this model is possible to obtain a gain higher than 20 dB and as has been said before typically an *EDFA* can achieve gains around 25 dB to 30 dB but it is important to have into account the fact the model under used is a noise-free model. Thus, the accuracy of the results obtained is limited to simulations where the gain per channel is inferior to 20 dB

2.7 Conclusions

In this chapter the general concepts for understanding and evaluating a transient were exposed. A group of parameters were defined to characterize a transient. These parameters are used to characterize time invariant linear systems, which typically may present an oscillatory time response. The amplifier (*EDFA*) is considered a system that for a certain input is possible to obtain a measurable output. However, to be considered a linear time invariant system has to fulfil the linear property (homogeneity and superposition) and invariance property. The amplifier response to an input power step respects the invariance property but does not respect the homogeneity and superposition property. Hence, the amplifier (*EDFA*) system is not a linear system, which does not invalidate the parameters chosen to evaluate the power transient, but justifies the non-existence of a linear relation between the parameters and the input power, and also other intrinsic *EDFA* characteristics.

Chapter 3. Transient Simulation in Optical Links

3.1 Introduction

To better expose the transient phenomenon, the *EDFA* model described in the previous chapter is used to simulate different possible scenarios. The novel parameters to describe a transient defined are used in this chapter to expose the differences between several results obtained in different simulation scenarios. This chapter aims to exhibit the transient dependency with the:

a. number of *EDFA*s chained;
b. input power per channel in the first *EDFA* of the chain;
c. number of channels dropped and added;
d. *EDFA* spectrum.

In order to expose these dependencies is important to assume before each simulation the *EDFA* intrinsic characteristics which are extracted from previous works. Changes on the intrinsic characteristics of the *EDFA*s, the cross-sections or the fiber length, are not the focus of this work.

The chapter starts in section 3.2 with two-channel scenarios in order to understand the transient dependency with (a) and (b). In section 3.3 the scenario is changed to an eleven *DWDM* signal. With this scenario the transient dependency with (a), (c) and (d) is exposed. The impact of a transient in the optical performance, according to the requirements imposed on section 2.4, is analyzed at the end of each simulation. The chapter ends with section 3.4 where the conclusions are summarized.

3.2 Two Channel Scenario with 980 nm Pump

3.2.1 Input Power of 3 dBm/Ch

The first considered case is identical to the one used in 2.6.2 and illustrated on Figure 2-15. The absorption coefficients are 0.257, 0.145, 0.125 m^{-1} and the intrinsic saturation powers are 0.440, 0.197, 0.214 mW at 980, 1552.1, 1557.7 nm, respectively. Using the parameters defined on section 2.2 the following results were obtained.

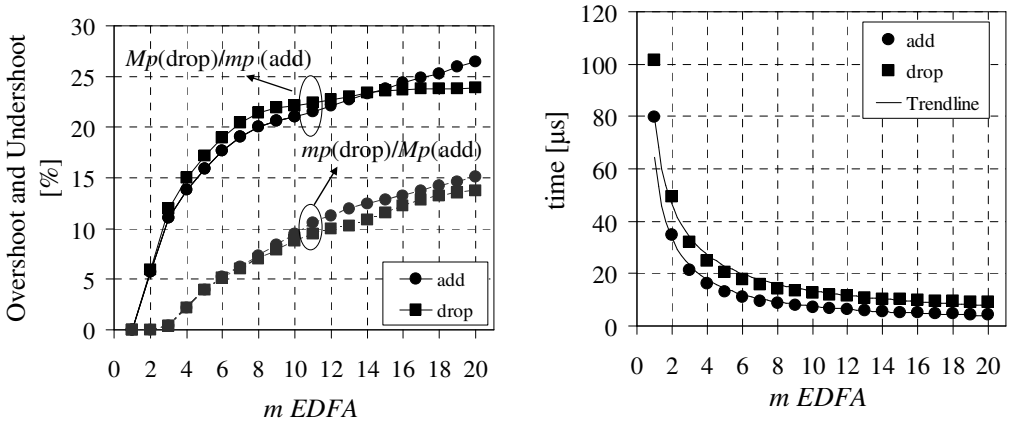

Figure 3-1 Channel 1 under analysis while channel 2 is dropped (2:1) and added (1:2); a) *Mp* and *mp* vs. *m* of *EDFA*s; b) *tr* vs. *m EDFA*s.

Figure 3-1 a) exposes the parameter *Mp* (overshoot) and *mp* (undershoot) dependency with the number of *EDFA*s in the link.

The power transient acquires an oscillatory response only after the second *EDFA*. Thus, *Mp* (drop) and *mp* (add) is zero at the first *EDFA*. The power transient acquires *Mp* (add) and *mp* (drop) after the third *EDFA*. Is possible to observe that the *Mp* and *mp* of the power transient increases with the number of *EDFA*s in the chain. This results from the cumulative effect of a rapid power transition on each *EDFA* combined with the power overshoot/undershoot of the previous *EDFA*. The *Mp* (drop) and the *mp* (add) curves have higher values, along the *EDFA* chain, than the *Mp* (add) and the *mp* (drop) curves. This results from cumulative effect of the reservoir transient, which leads to a 2^{nd} order behaviour of the power transient. Note that the *Mp* (drop) saturates faster than the *mp* (add) with the *EDFA* count. In a two-channel scenario, when one is dropped, all available pump power is distributed to one

surviving channel. The new static gain for the surviving channel depends on the intrinsic *EDFA* characteristic and the pump power, which leads to a "faster" output power saturation of the surviving channel with the increase of the *EDFA* count. When one channel is added, the available pump power has to be re-distributed for two channels leading a re-adjustment of the output power from *EDFA* to *EDFA*, which results in a "slower" increase of the *mp* (add) with the *EDFA* count.

There is a similar behaviour between *Mp* (drop) and *mp* (add) and also between *Mp* (add) and *mp* (drop). This correlation was expected since the definition of this parameter is the same for a channel add/drop and the power transient after a channel add has the inverse behaviour than the power transient of a channel drop.

Note that the rate of increase of all the considered parameters in Figure 3-1 a) decreases significantly when the amplifier count is above 7. This results from the limited power interval, due to gain saturation, at the output of each *EDFA*, which restricts the growth of the overshoot/undershoot. For this reason, it is expected that the behaviour of these parameter is non-monotonous. This effect will be shown in chapter 4 with experimental results.

The requirements defined in section 2.4 for overshoot, requirement of 26% maximum in a drop, is achieved in this simulation. The *Mp* (drop) achieves a maximum of 24%. The requirement of undershoot inferior to 26% in a channel add scenario is achieved at the twentieth *EDFA* of the link. The *mp* (add) achieves a maximum of 26.5%.

Figure 3-1 b) shows the parameter *tr* dependency with the number of *EDFA*s. The rise time and the fall time of the power transient response, when a channel is dropped or added, decreases with the number of *EDFA*s in the chain. This shows that, similarly to the overshoot the cumulative effect of the power transition with transients from previous *EDFA*s tend to increase the speed of the transient. The decrease of *tr* (drop/add) may be empirically estimated by the following approximation:

$$tr_{drop}(m) \approx \frac{79.5}{m^{0.8}}, \quad 1 \le m \le 20 \quad [\mu s] \tag{3.1}$$

and

$$tr_{add}(m) \approx \frac{64.2}{m^{0.9}}, \quad 1 \le m \le 20 \quad [\mu s]. \tag{3.2}$$

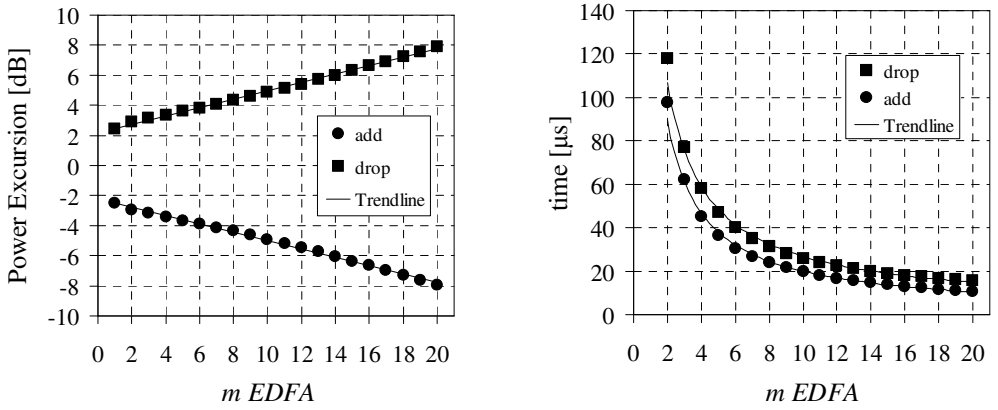

Figure 3-2 Channel 1 under analysis while channel 2 is dropped (2:1) and added (1:2); a) Power Excursion at *tr* vs. *m EDFA*s; b) Peak time (*tp*) vs. *m EDFA*s.

Figure 3-2 a) exposes the power excursion at rise/fall time (*tr*) which also exhibits an approximately linear behaviour with an increase/decrease of +/- 0.28dB/*EDFA*.The power excursion associated to a drop is similar in absolute value to an add. Hence, it is symmetrical through the number of *EDFA*s in a logarithmic scale. A linear regression applied to Figure 3-2 b) curves, results in:

$$Pe_{tr}(m) = \pm 0.28\, m \pm 2.2, \quad 1 \le m \le 20 \quad [dB]\ . \tag{3.3}$$

Figure 3-2 b) exhibits the *tp* dependency with the number of *EDFA*s on the link. The results are in agreement with Figure 3-1 b) and shows that the power transient response when channels are added achieves its minimum value faster than when channels are added. The difference between *tp* (drop) and *tp* (add) decreases with the number of *EDFA*s and there is no *tp* after the first EDFA since there is no overshoot or undershoot. After the second *EDFA* is the difference between *tp* (drop) and *tp* (add) is of 19.9 µs and reduces to 14.7 µs after the third *EDFA*. After the seventh *EDFA* the difference is 8 µs and after twenty *EDFA*s is 4.9 µs. For the *tp*, within a margin of 1 µs, the difference remains approximately constant after thirteenth *EDFA*. Figure 3-2 b) exhibits approximation curves to *tp* (drop) and *tp* (add) with decay analogous to *tr*, given by:

$$tp_{drop}(m) \approx \frac{194.3}{m^{0.7}}, \quad 2 \le m \le 20 \quad [\mu s], \tag{3.4}$$

and

$$tp_{add}(m) \approx \frac{170.5}{m^{0.9}}, \quad 2 \le m \le 20 \quad [\mu s]. \tag{3.5}$$

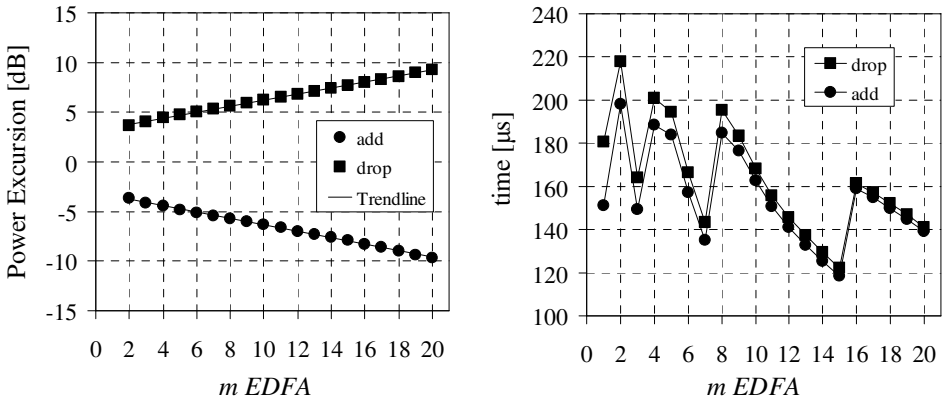

Figure 3-3 Channel 1 under analysis while channel 2 is drop/add (2:1/1:2): a) Power excursion at *tp* vs. *m EDFA*s; b) Settling time vs. *m EDFA*s.

Is also possible to observe from Figure 3-3 a) that the Pe_{tp} has an approximately linear increase/decrease of +/- 0.3 dB/*EDFA*, in logarithmic units, which leads to the following linear regression:

$$Pe_{tp}(m) \approx \pm 0.3m \pm 3.2, \quad 2 \le m \le 20 \quad [dB]. \tag{3.6}$$

Figure 3-3 b) shows the settling time of the power transient response dependency with the number of *EDFA*s on the link. The margin given was of 2% and according to Figure 3-3 b), the settling time decreases with the number of *EDFA*s. However, since the power oscillations increase from *EDFA* to *EDFA*, an oscillation that in the previous *EDFA* was inferior to 2% after the next *EDFA* can become superior to 2%. This behaviour is exposed after the second, the fourth, eighth and after the sixteenth *EDFA*, when a channel is dropped and the sixteenth when is added. To exclude the possibility of a precision error the number of samples used in the simulation of a power transient was increased in ten times to reduce the precision error and the results remained the same. Although the *ts* has a non-linear behaviour, is possible to observe that *ts* (add) curve is below *ts* (drop) curve. Thus, *ts* (add) is faster than *ts* (drop) which is in agreement with the results obtained for *tr* and *tp*. After the first *EDFA* the

difference between the two curves is 29.4 μs and it reduces to 20.4 μs after the second. After the seventh is 8 μs, after the tenth *EDFA* is 5.3 μs and finally after the twentieth *EDFA* is 1.8 μs. Is possible, to observe a reduction in the difference between the *ts* (drop) and *ts* (add).

Figure 3-4 exhibit the *SR* when a channel is dropped and when a channel is added. The *SR* (drop) is empirically interpolated by a linear regression, in logarithmic units, which increases with the number of *EDFA*s in the chain.

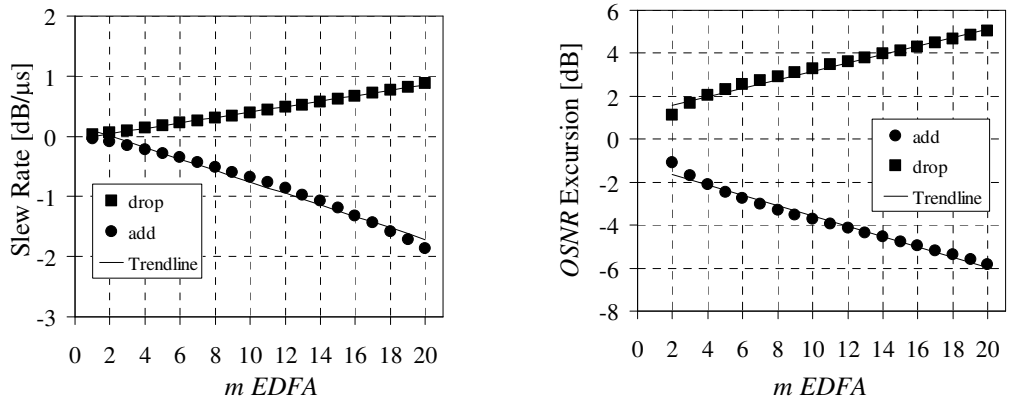

Figure 3-4 Channel 1 under analysis while channel 2 is drop/add (2:1/1:2): a) Slew rate (*SR*) in a chain of 20 *EDFA*s; b) OSNR excursion at *tp* in a chain of 20 *EDFA*s.

The *SR* (add) is empirically interpolated by linear regression but is possible to observe that the decreasing behaviour of the curve is not linear. This results from $Pe(tr)_{\text{drop}} \approx Pe(tr)_{\text{add}}$ and *tr* (add) > *tr* (drop), which decreases with the number of *EDFA*s in the chain. Thus, for this simulation, the *SR* interpolation is given by:

$$SR(m) \approx \begin{cases} 0.045m - 0.047 & (drop) \\ -0.096m + 0.019 & (add) \end{cases}, \quad 1 \le m \le 20 \quad [dB/\mu s]. \tag{3.7}$$

The slew rate requirement to ensure an effective response of the *AGC* in the optical receiver is of 0.5 dB/μs. Analyzing Figure 3.4 a) is possible to infer that the threshold is crossed at the thirteenth *EDFA* for the drop channel scenario and at the eighth *EDFA* for the channel add scenario.

The worst case of *OSNR* excursion occurs at power transient peak instant, thus the focus of this simulation is the $OSNRe_{tp}$ exposed on Figure 3-4 b). The result exposed on Figure 3-4 b) and is empirically approximated using a linear interpolation as:

$$OSNRe(m) \approx \pm 0.2\,m \pm 1.2, \quad 2 \le m \le 20 \quad [dB], \tag{3.8}$$

where *m* is the *EDFA* count and + signal is chosen in case of a drop and the - in case of an add. The requirement for *OSNRe* at *tp* instant is a maximum of 3dB. This threshold is crossed at the tenth *EDFA* for a channel drop and at the eighth *EDFA* for a channel add scenario. This result can be inferred from Figure 3-4 b).

3.2.2 Input Power per Channel

The second numerical example is the similar to the previous one but with a variable input power per channel. The amplifier has two input channels λ_1 = 1552.1 nm, λ_2 = 1557.7 nm, with initial input powers of 3dBm/Ch, -10dBm/Ch and -20 dBm/Ch. The amplifier is pumped at 980 nm, with pump power of 18.4 dBm, and has *L* = 35 m. This simulation focuses on power transients that result from the drop of channels.

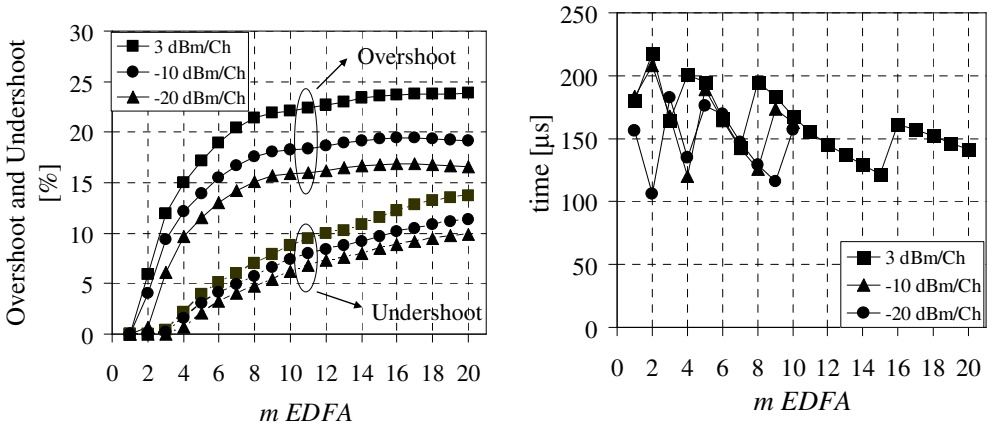

Figure 3-5 Channel 1 under analysis while channel 2 is drop (2:1): a) Overshoot and Undershoot vs. *m EDFA*s; b) Settling time vs. *m EDFA*s.

From Figure 3-5 a) exposes the *Mp* and *mp* dependency with the input power per channel at the input of the first *EDFA* ($P^{in}_{j,1}$). Figure shows that the overshoot decreases when $P^{in}_{j,1}$ reduces and this decrease is more significant for *Mp*.

Figure 3-5 b) exposes settling time (*ts*) parameter dependency with the number of *EDFA*s and with $P^{in}_{j,1}$. The behaviour of *ts* curves with different $P^{in}_{j,1}$ are similar after the fifth *EDFA*. As has been said before, when the number of *EDFA*s increases some power transient oscillations that were within a margin of 2% on a previous *EDFA* on the next may pass the given margin. With a decrease of $P^{in}_{j,1}$ the m^{th} *EDFA* at which the power transient oscillations pass the 2% margin increases. Thus, *ts* has increasing time peaks after a different number of *EDFA*s.

As an example let's analyze *ts* behaviour between the seventh and the eleventh *EDFA*. After the seventh *EDFA,* with different $P^{in}_{j,1}$, *ts* has the same value of approximately 140 µs. With $P^{in}_{j,1}$ of 3dBm/Ch after the eighth *EDFA* there is an increase on *ts.* However, with -10dBm/Ch the increase on *ts* occurs after the ninth *EDFA*. This increase brings up *ts* (-10dBm/Ch) to the same value of *ts* (3dBm/Ch). Using -20dBm/Ch the increase in *ts* occurs after the tenth *EDFA*. At this point, with different $P^{in}_{j,1}$ the *ts* has approximately the same value of 160 µs.

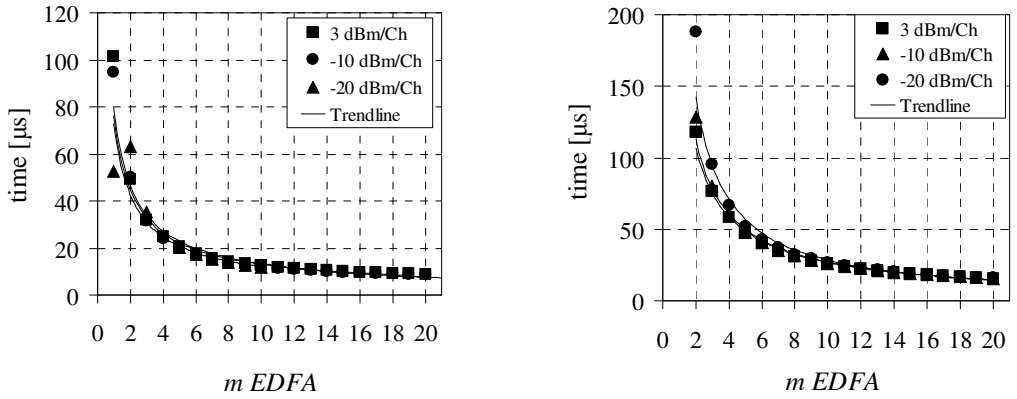

Figure 3-6 Channel 1 under analysis while channel 2 is drop (2:1). Simulation with 3dBm/Ch, -10dBm/Ch, -20dBm/Ch: a) Rise time vs. *m EDFA*s; b) Peak time vs. *m EDFA*s.

Figure 3-6 a) and b) exposes the rise time (*tr*) and the peak time (*tp*) respectively. From both figures is possible to extract that $P^{in}_{j,1}$ has no significant impact on *tr* and *tp* except after the first *EDFA*. Using 3dBm/Ch *tr* has approximately the same value of 100 µs (102µs respectively) and with -20dBm/Ch has less 50 µs. Thus, the power transient response becomes faster after the first *EDFA* with the decrease of $P^{in}_{j,1}$.

After the first *EDFA* the values of *tr* and *tp* converge rapidly for the same value with the increase of the number of *EDFA*s for the different $P^{in}_{j,1.}$ This result from the fact that the total output power converges to the same value, and because the span

attenuation is constant, the total input power after the first *EDFA* converges to the same value at the input of the following *EDFA*s of the chain.

On the other hand, *tp* becomes slower after the first *EDFA* when $P^{in}_{j,1}$ decreases. From Figure 3-6 b) is possible to extract that with -20dBm/Ch *tp* is approximately 187.8 μs and with a higher $P_{j,1}$ of 3dBm/Ch *tp* is around 117.7 μs, which is a difference of 70.1 μs. In addition, *tr* and *tp* have the following behaviour:

$$tr(m) \approx \frac{tr_0}{m^{0.8}}, \quad 1 \le m \le 20 \quad [\mu s], \tag{3.9}$$

where *m* is the *EDFA* count and tr_0 is [79.5; 72.8; 76.2] for [3; -10; -20] dBm/Ch, respectively. For the peak time (*tp*) the curve has the following approximation:

$$tp(m) \approx \frac{tp_0}{m^{x}}, \quad 2 \le m \le 20 \quad [\mu s], \tag{3.10}$$

where *m* is the *EDFA* count, tp_0 is 194.3, 208.5, 285.6 μs and *x* is 0.9, 0.9, 1.0 for 3, -10, -20 dBm/Ch, respectively.

From Figure 3-7 is possible to infer the behaviour of power excursion at *tr* and at *tp*, a) and b) respectively. Both figures expose a linear behaviour with a decrease on the power excursion with the decrease of the input power. The offset between 3dBm/Ch and -20 dBm/Ch is around 1.1dB for Pe_{tr} with an increase rate of approximately 0.26dB/*EDFA*. Thus, Pe_{tr} has approximately the following behaviour:

$$Pe_{tr}(m) \approx 0.26\,m + 2.2 - \left[P^{3dBm}_{ref} - P^{in}_{j,1}\right]0.05, \quad 1 \le m \le 20 \quad [dB]. \tag{3.11}$$

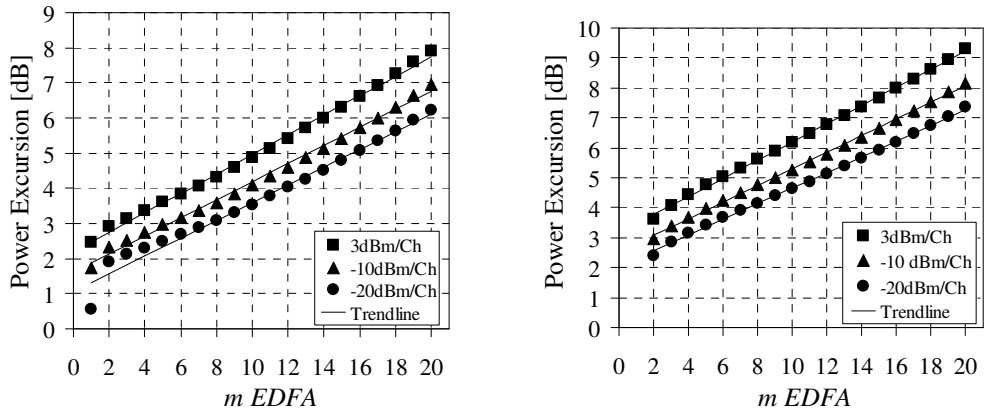

Figure 3-7 Channel 1 under analysis while channel 2 is drop (2:1). Simulation with 3 dBm/Ch, -10 dBm/Ch, -20 dBm/Ch: a) Pe_{tr} vs. m *EDFA*s; b) Pe_{tp} vs. *m EDFA*s.

The offset between 3dBm/Ch and -20 dBm/Ch is around 1.2dB for Pe_{tr} with an increase rate of approximately 0.26dB/*EDFA*. Thus, Pe_{tp} has approximately the following behaviour:

$$Pe_{tp}(m) \approx 0.26\,m + 3.2 - \left[P_{ref}^{3dBm} - P_{j,1}^{in}\right]0.05, \quad 1 \le m \le 20 \quad [dB]. \tag{3.12}$$

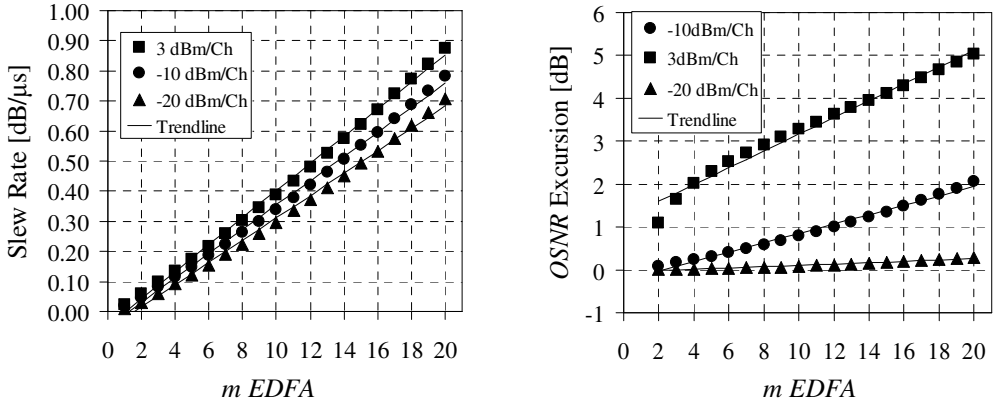

Figure 3-8 Simulation with 3 dBm/Ch, -10 dBm/Ch, -20 dBm/Ch: a) Slew rate (*SR*) in a chain of 20 *EDFA*s; b) *OSNR* excursion at instant *tp*.

Figure 3-8 a) exhibits the *SR* in a channel drop scenario, when $P^{in}_{j,1}$ decreases. It is possible to observe a decrease in the *SR* with the decrease of $P^{in}_{j,1}$. The slew rate dependency with the *EDFA* count increases with the reduction $P^{in}_{j,1}$. The *SR* of a channel-drop scenario is approximately linear which leads to, for $P^{in}_{j,1}$ = 3dBm/Ch,

$$SR_{drop}(m) \approx 0.044\,m - 0.044, \quad 1 \le m \le 20 \quad [dB/\mu s], \tag{3.13}$$

and for $P^{in}_{j,1}$ = -20dBm/Ch, leads to:

$$SR_{drop}(m) \approx 0.036\,m - 0.057, \quad 1 \le m \le 20 \quad [dB/\mu s]. \tag{3.14}$$

Analyzing Figure 3-8 a) is possible to infer that the threshold is crossed at the fourteenth *EDFA* for the -10 dBm/Ch and after the sixteenth *EDFA* for the -20 dBm/Ch.

The result exposed on Figure 3-8 b) and is empirically approximated using a linear interpolation as:

$$OSNR_e(m) \approx 0.1m - 0.2, \quad 2 \le m \le 20 \quad [dB], \tag{3.15}$$

for $P^{in}_{j,1}$ = -10dBm/Ch, and

$$OSNR_e(m) \approx 0.02m - 0.05, \quad 2 \le m \le 20 \quad [dB], \tag{3.16}$$

for $P^{in}_{j,1}$ = -20dBm/Ch where *m* is the *EDFA* count.

Analyzing Figure 3-8 b) is possible to infer that the threshold is not crossed in a chain of 20 *EDFA*s for -10 dBm/Ch and -20dBm/Ch.

3.3 *DWDM* Signal with 980 nm Pump

The following simulation has as main goal to analyze the power transients on a *DWDM* signal. Thus, based on the work of Pachinke, S. *et al.* [26] the same *EDFA* intrinsic characteristics were used to simulate a *DWDM* signal.

Ch #	**1**	**2**	**3**	**4**	**5**	**6**	**7**
[*THz*]	306.1	192.1	192.2	192.5	192.7	192.8	192.9
[*nm*]	980	1560.606	1559.794	1557.363	1555.747	1554.940	1554.134
α_j [m^{-1}]	0.3	0.105	0.105	0.113	0.116	0.117	0.118

$P_j^{IS}[mW]$	1.5	0.365	0.365	0.350	0.339	0.330	0.322

Ch #	8	9	10	11	12
[*THz*]	193.0	193.1	193.2	193.4	193.5
[*nm*]	1553.329	1552.524	1551.721	1.550.116	1.549.315
$\alpha_j\,[m^{-1}]$	0.117	0.12	0.123	0.123	0.123
$P_j^{IS}[mW]$	0.320	0.316	0.31	0.308	0.304

Table 2 – Measured *EDFA* parameters for a *DWDM* signal.

Table 2 exposes measured values for absorption coefficients α_j and the intrinsic saturations powers P_j^{IS}. These values have been measured experimentally at Pachinke, S. *et all* work. The absorption coefficients can be determined by monochromatic measurement of small-signal transmission, and the intrinsic saturation power is defined as the power level where the attenuation is bleached by a factor of *e* (=4.34dB).

3.3.1 The Drop vs. Add in a *DWDM* Optical Link

The simulation scenario from Figure 3-9 is used to simulate an 11:1 and 1:11 channel drop and add respectively. At instant $t=0^+$, channels from λ_2 to λ_{12} are dropped and added with the exception of λ_7. Using the *EDFA* intrinsic characteristics exposed on Table 2, with initial input power of -15dBm/Ch and an interamplifier attenuation fixed of 20dB. The amplifier is pumped at 980 nm, with pump power of 18.4 dBm, and has L = 35 m. The chain is composed by m *EDFA*s.

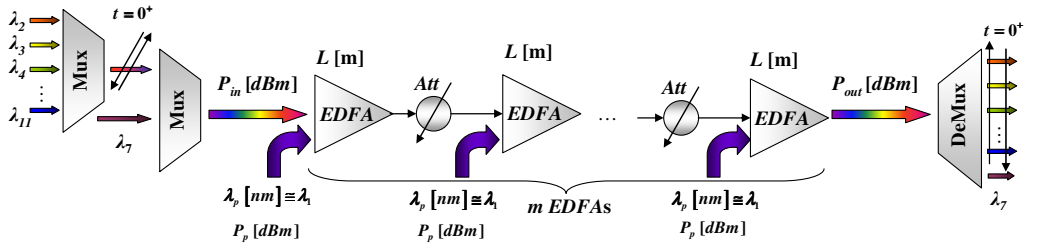

Figure 3-9 Simulation of a *DWDM* optical link of 11 channels with 980 nm pump signal.

The following results have been obtained for channel λ_7. Figure 3-10 illustrates the power transient after ten channels of an eleven-channel *DWDM* signal are dropped in a chain of 10 *EDFA*s.

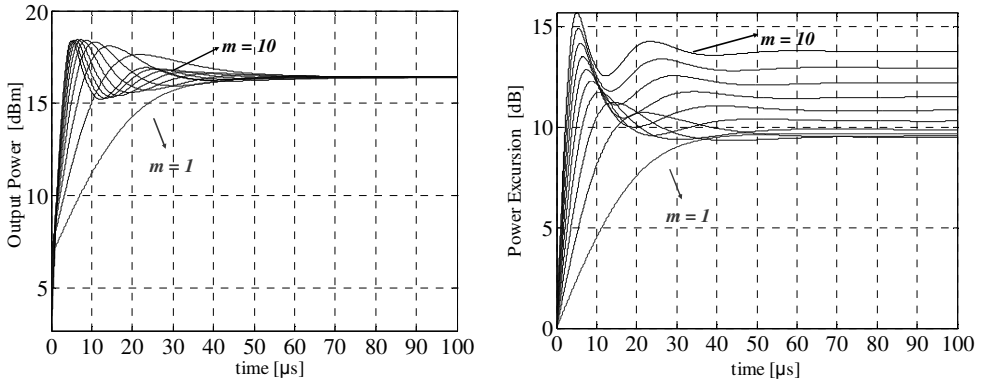

Figure 3-10 Channel drop from 11:1 with 18.4 dBm of pump power, *L* = 35m and a span attenuation of 20 dB a) Output Power of channel λ_7 b) Power Excursion of channel λ_7.

On Figure 3-10 a) the output power after the m^{th} *EDFA* of the surviving channel λ_{12} is plotted. On Figure 3-10 b) the power excursion of channel λ_7, after the m^{th} *EDFA* is illustrated.

It is possible to observe qualitatively that the channel power excursion increases with the number of *EDFA*s on the optical link. The $P_{out}(ts)$ is approximately the same after each *EDFA* and Pe_{ts} increases with the *EDFA* count. This results from the fact that $P_{out}(0^-)$ reduces with the EDFA count due to the achievement of the *EDFA* saturation and the constant 20 dB of attenuation.

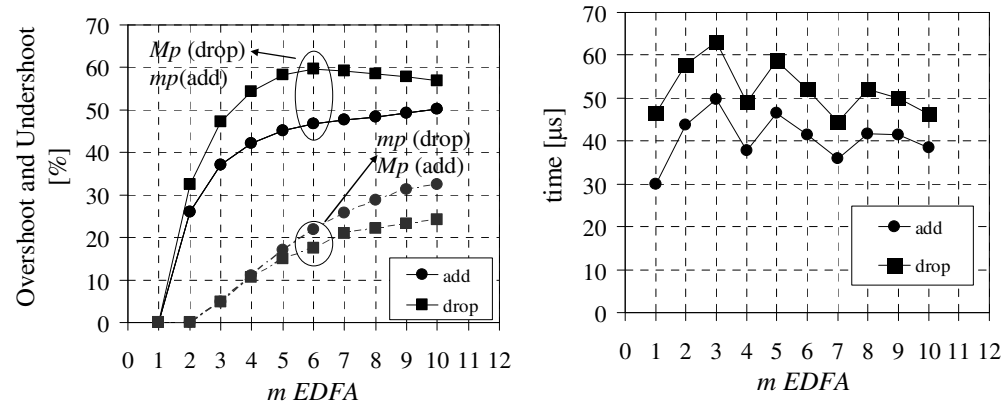

Figure 3-11 Channel drop/add from 11:1 and 1:11, respectively: a) *Mp* and *mp* vs. *m EDFA*s for channel λ_7 b) *ts* vs. *m EDFA*s for channel λ_7.

Figure 3-11 illustrates the overshoot and undershoot dependency with the number of *EDFA*s for channel λ_{12}. The figure exhibits a higher *Mp* (drop) than an *mp* (add). It shows that *Mp* (drop) curve has a maximum value at the sixth *EDFA* (approximately 60%) and decreases after the eighth. The *mp* (add) achieves a maximum of approximately 37.2% on the tenth *EDFA*. This behaviour is different from the one

observed in Figure 3-1 where *Mp* curve converge to a maximum value but do not expose decrease behaviour after achieving it. The *mp* (add) curve has an increasing behaviour which is a similar behaviour exposed on Figure 3-5 a) achieving a saturation value. After the tenth *EDFA* the *mp* (drop) curve has a difference of 8.3% from *Mp* (add).

Figure 3-11 b) illustrates the settling time which has also a similar to the one exposed on Figure 3-3 b). The *ts* (add) curve exhibits lower values than the *ts* (drop), which is coherent with the results obtained before. The two curves exhibit a similar behaviour and the difference between both reduces with the increase of the number of *EDFA*s. After the first *EDFA* is approximately 6.3 μs and after the tenth is of 7.8 μs.

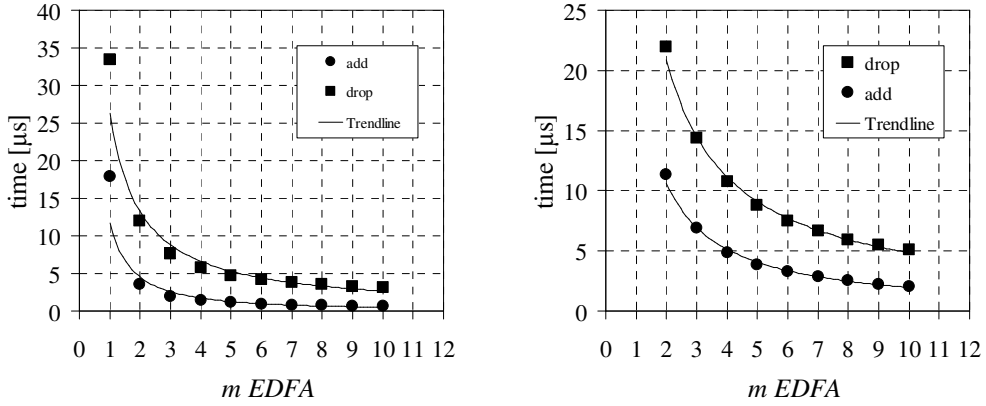

Figure 3-12 Channel drop/add from 11:1 and 1:11, respectively: a) *tr* vs. *m EDFA*s for channel λ_7 b) *tp* vs. *m EDFA*s for channel λ_7.

For *tr* and *tp* parameter from Figure 3-12 is possible to infer an identical decay behaviour to the one observed in Figure 3-6. Figure 3-12 a) exposes *tr* dependence with the *m*. The *tr* (drop) curve may be empirically approximated using a power interpolation as:

$$tr(m) \approx \frac{33.4}{m}, \quad 1 \le m \le 10, \quad [\mu s], \tag{3.24}$$

where, *m* is the amplifier count. In the case of channel add, this relation becomes:

$$tr(m) \approx \frac{17.6}{m^{1.4}}, \quad 1 \le m \le 10, \quad [\mu s]. \tag{3.25}$$

Figure 3-12 b) exhibits the *tp* dependency with *m*. The *tp* (drop) curve may be empirically approximated using a power interpolation as:

$$tp(m) \approx \frac{39.2}{m}, \quad 2 \le m \le 10, \quad [\mu s], \tag{3.26}$$

where, *m* is the amplifier count. In the case of channel add, this relation becomes:

$$tp(m) \approx \frac{21.9}{m}, \quad 2 \le m \le 10, \quad [\mu s]. \tag{3.27}$$

Expressions (3.24) to (3.27) provide a simple estimate of the *tr* and *tp* variation with the number of amplifiers in the chain.

The power excursion curves associated to *tr* and *tp* are illustrated on Figure 3-13. Both figures a) and b) expose the increase in the power excursion.

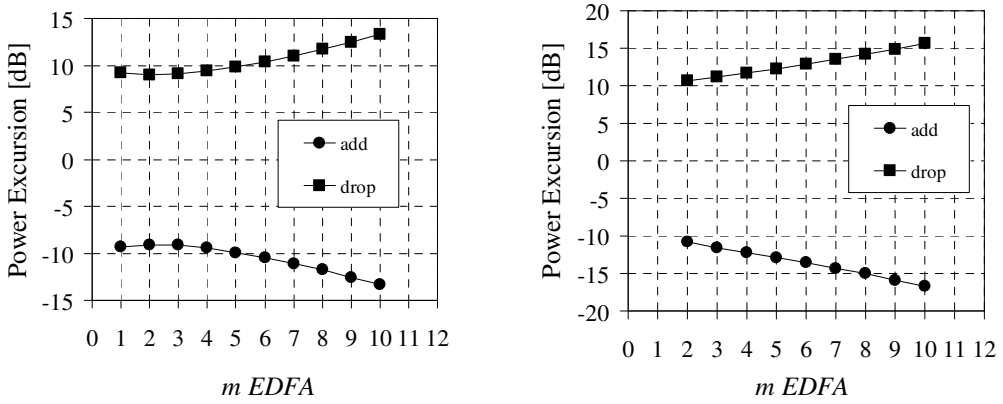

Figure 3-13 Channel drop/add from 11:1 and 1:11, respectively: a) Power Excursion at *tr* vs. *m EDFA*s for channel λ_7; b) Power Excursion at *tp* vs. *m EDFA*s for channel λ_7.

For Pe_{tr} the decay is empirically rough approximated using a linear interpolation as:

$$Pe_{tr}(m) \approx \pm 0.5\, m \pm 7.9, \quad 1 \le m \le 10, \quad [dB], \tag{3.28}$$

for the Pe_{tp} the decay may be also empirically rough approximated using a linear interpolation as:

$$Pe_{tp}(m) \approx \pm 0.6\, m \pm 9.3, \quad 2 \le m \le 10, \quad [dB]. \tag{3.29}$$

For both expressions, (3.28) and (3.27), in case of a channel drop the signal combination is + and +. In case of a channel add, the signal combination is - and -. The variable *m* is the amplifier count.

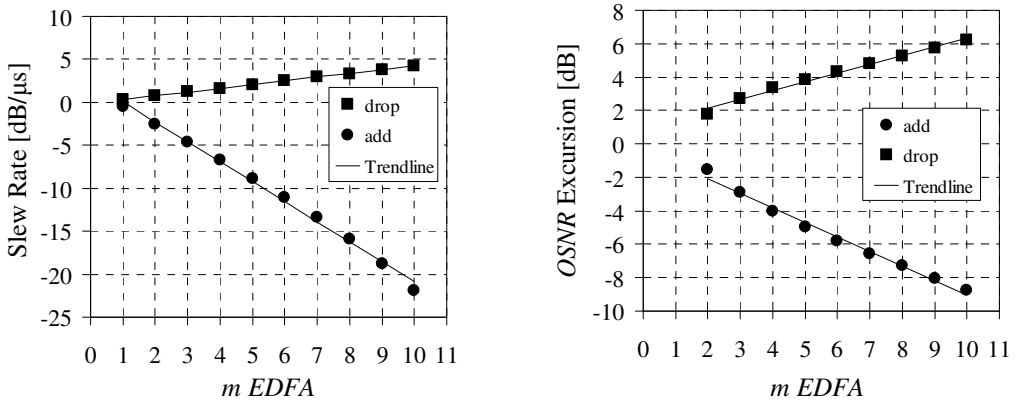

Figure 3-14 Channel drop/add from 11:1 and 1:11, respectively: a) Slew rate (*SR*) in a chain of 10 *EDFA*s; b) *OSNR* excursion at instant *tp*.

Figure 3-14 a) exhibits the *SR* in a 11:1 channel drop and in a 1:11 add scenario. The *SR* of a channel-drop/add scenario is approximately linear which leads to:

$$\begin{aligned} SR_{drop}(m) &\approx 0.44\,m - 0.13, \quad 1 \le m \le 20 \quad [dB/\mu s] \\ SR_{add}(m) &\approx -2.33\,m + 2.39, \quad 1 \le m \le 20 \quad [dB/\mu s] \end{aligned}, \tag{3.13}$$

where *m* is the *EDFA* count. Analyzing Figure 3-14 a) is possible to infer that the threshold is crossed after the second *EDFA* for the 11:1 channel drop scenario and also after the second *EDFA* for the 1:11 channel add scenario. This results leads to a limitation of 1 *EDFA* in a link with a 11 channel *DWDM* signal.

The result exposed on Figure 3-14 b) and is empirically approximated using a linear interpolation as:

$$\begin{aligned} OSNRe(m) &\approx 0.52m + 1.09, \quad 2 \le m \le 20, \quad \textit{11:1 drop} \quad [dB] \\ OSNRe(m) &\approx -0.87m - 0.29, \quad 2 \le m \le 20, \quad \textit{1:11 add} \quad [dB] \end{aligned}, \tag{3.15}$$

where *m* is the *EDFA* count. Analyzing Figure 3-14 b) is possible to infer that the 3dB threshold is crossed after the fourth *EDFA*.

3.3.2 The Power Transient Spectral Dependency

The intrinsic characteristics of the *EDFA* dependency with wavelength are exposed on Table 2. Is important to understand the power transient dependency with wavelength since the gain experience by each channel depends on the gain coefficient and of *EDFA* length. Thus, the drop of 11:1 channel, where the surviving channel is variable between λ_{10}, λ_{11} and λ_{12}, is simulated according to Figure 3-15.

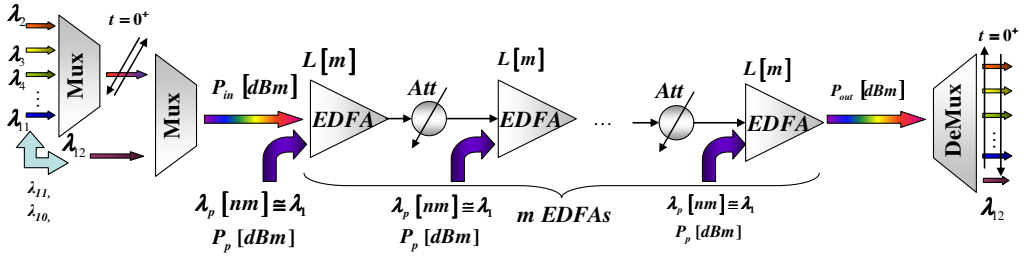

Figure 3-15 – DWDM simulation setup of an 11:1 channel drop with a variable surviving channel.

Figure 3-16 a) exposes the *Mp* and *mp* of an eleven channel drop to a single surviving channel after a chain of ten *EDFA*s.

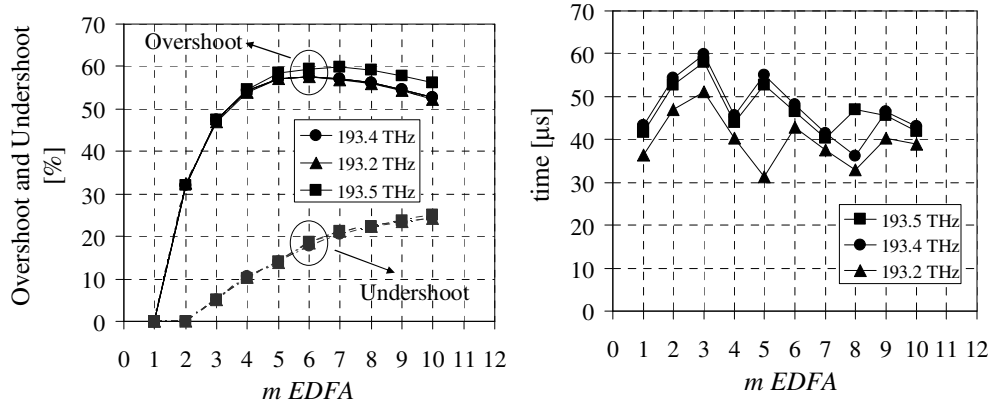

Figure 3-16 Channel drop from 11:1: a) Overshoot and undershoot vs. *m EDFA*s for channel λ_{12}, λ_{11} and λ_{10}; b) Settling time vs. *m EDFA*s for channel λ_{12}, λ_{11} and λ_{10}.

It is possible to observe differences when the surviving channel has a different frequency. For each surviving channel the maximum *Mp* occurs after the sixth *EDFA*. The *mp* is similar for the different surviving channels. Thus, changing the surviving channel does not have significantly impact on the overshoot and undershoot.

Figure 3-16 b) exposes *ts* for different surviving channels. The behaviour of *ts* with the number *EDFA*s on the optical link is similar to the ones presented on previous simulations (e.g. Figure 3-11 b)). From Figure 3-16 b) is possible to infer that until the fourth *EDFA* the different *ts* curves exhibit similar values with a maximum difference of 8 μs. After the fifth *EDFA* the $ts(\lambda_{10})$ exhibit a lower value than $ts(\lambda_{11})$ and $ts(\lambda_{12})$, with a difference of 17 μs. However, after the sixth *EDFA* until the tenth the power transient exposes similar *ts* values.

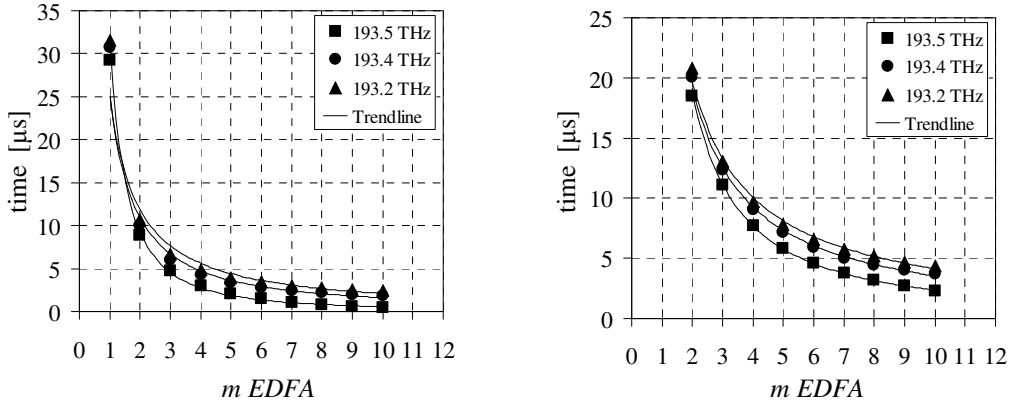

Figure 3-17 Channel drop from 11:1 for channel λ_{12}, λ_{11} and λ_{10}: a) Rise time vs. *m EDFA*s; b) Peak time vs. *m EDFA*s.

Figure 3-17 a) illustrates the rise time for the different surviving wavelengths. It is possible to infer the same behaviour already exposed on Figure 3-16 b), the $tr(\lambda_{12})$ behaviour with the number of *EDFA*s is faster than $tr(\lambda_{11})$ and $tr(\lambda_{11})$ is faster than $tr(\lambda_{10})$. Between $tr(\lambda_{10})$ and $tr(\lambda_{11})$ after the first *EDFA* there is a difference of approximately 1 μs and after ten *EDFA*s the difference maintains around the 1 μs. The *tr* curves may be empirically approximated using a power interpolation as:

$$
\begin{aligned}
tr(m) &\approx \frac{31.3}{m^{1.8}}, \quad 1 \le m \le 10, \quad f = 193.5THz \quad [\mu s]; \\
tr(m) &\approx \frac{25}{m^{1.2}}, \quad 1 \le m \le 10, \quad f = 193.4THz \quad [\mu s]; \\
tr(m) &\approx \frac{25}{m^{1.1}}, \quad 1 \le m \le 10, \quad f = 193.2THz \quad [\mu s],
\end{aligned}
\tag{3.16}
$$

the variable *m* is the amplifier count.

Figure 3-17 b) exposes the *tp* dependency with the number of *EDFA*s and with wavelength.. For *tp* the difference between $tp(\lambda_{10})$ and $tp(\lambda_{11})$ after the first *EDFA* is of approximately 10 µs and after ten *EDFA*s reduces to a difference of approximately 5µs. The *tp* curves may be empirically approximated using a power interpolation as:

$$tp(m) \approx \frac{45.8}{m^{1.3}}, \quad 2 \le m \le 10, \quad f = 193.5THz \quad [\mu s];$$
$$tp(m) \approx \frac{39.6}{m^{1.1}}, \quad 2 \le m \le 10, \quad f = 193.4THz \quad [\mu s]; \qquad (3.17)$$
$$tp(m) \approx \frac{38.5}{m^{1}}, \quad 2 \le m \le 10, \quad f = 193.2THz \quad [\mu s],$$

the variable *m* is the amplifier count.

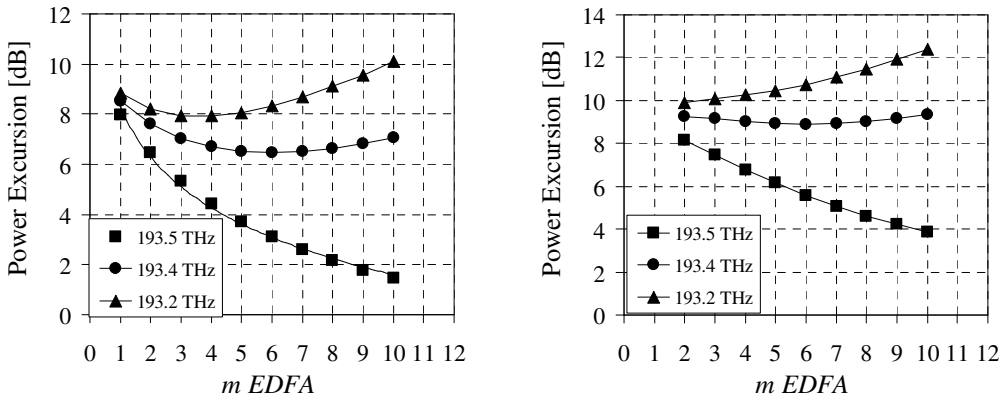

Figure 3-18 Channel drop from 11:1 for channel λ_{12}, λ_{11} and λ_{10}: a) Power Excursion at *tr* vs. *m EDFA*s; b) Power Excursion at *tp* vs. *m EDFA*s.

Figure 3-18 illustrates the power excursion at *tr* and *tp*, a) and b) respectively. A change in the behaviour of the curves form a decrease to an increase can be observed and also an increase on the offset of both figures. This results from the fact that the attenuation is constant and the *EDFA* saturation is wavelength dependent. For λ_{12} and λ_{11} the saturation is not achieved at the input of each *EDFA* which leads to a increase of the $P_{out}(0^-)$. After the drop, all the *Pp* available is distributed by surviving channel, λ_{12} or λ_{11} that rises its power until $P_{out}(ts)$ which is approximately the same after m^{th} *EDFA*. Hence, the $P_{out}(0^-)$ increases and $P_{out}(ts)$ remains equal with the increase of the number of *EDFA*s in the chain, this leads to a reduction of *Pe*. For λ_{10} the saturation is achieved leading to a *Pe* increase. Thus, depending of the channel that is under analysis, the power excursion dependency with the number of *EDFA*s has not an

obligatory increasing behaviour. However, typically in network planning, the *EDFA*s are saturated to reduce the *NF*. Thus, the power transient changes from surviving wavelength to surviving wavelength, being the impact of this variable more significant for the power excursion than for the time parameters since the spectral characteristics of *EDFA* define the gain coefficient for each wavelength.

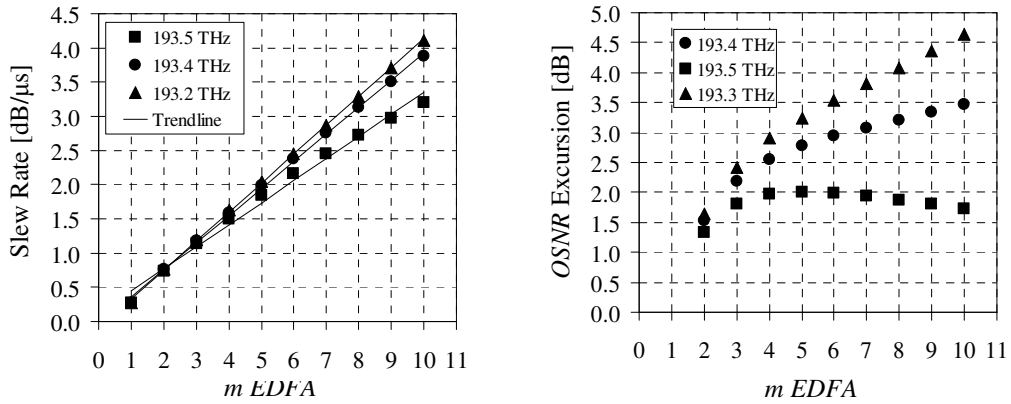

Figure 3-19 Channel drop from 11:1 for channel λ_{12}, λ_{11} and λ_{10}: a) Slew Rate vs. *m EDFA*s; b) *OSNR* Excursion at *tp* vs. *m EDFA*s.

Figure 3-19 a) exhibits the *SR* in a 11:1 channel drop for λ_{12} (193.5 THz) λ_{11} (193.4 THz) and λ_{10} (193.3 THz). The *SR* of a channel-drop/add scenario is approximately linear which leads to:

$$\begin{aligned} SR_{193.5\,\mathrm{THz}}(m) &\approx 0.32m - 0.13, \quad 1 \le m \le 20 \quad [dB/\mu s] \\ SR_{193.4\,\mathrm{THz}}(m) &\approx 0.39m - 0.03, \quad 1 \le m \le 20 \quad [dB/\mu s], \\ SR_{193.2\,\mathrm{THz}}(m) &\approx 0.42\,m - 0.09, \quad 1 \le m \le 20 \quad [dB/\mu s] \end{aligned} \tag{3.18}$$

where *m* is the *EDFA* count. Analyzing Figure 3-19 a) is possible to infer that the threshold is crossed after the second *EDFA* for all channels. Analyzing Figure 3-19 b) is possible to infer that the 3dB threshold is crossed after the fourth *EDFA* for 193.2 THz and after the seventh for 193.4 THZ. For channel 193.5 is threshold is not crossed in a chain of 10 *EDFA*s.

3.3.3 The drop of 11 to *n* channels in cascade of *EDFA*s

In the following simulation the dependency with the number of channels that are dropped or added in an 11 channel system is exposed. The setup from
Figure 3-20 is used to simulate an 11:*n* and *n*:11 channel drop and add respectively. Using *EDFA* intrinsic characteristics from Table 2 and with initial input powers of -15 dBm/Ch. The amplifier is pumped at 980 nm, with pump power of 18.4 dBm, and *L* = 35 m, has 20 dB of span attenuation.

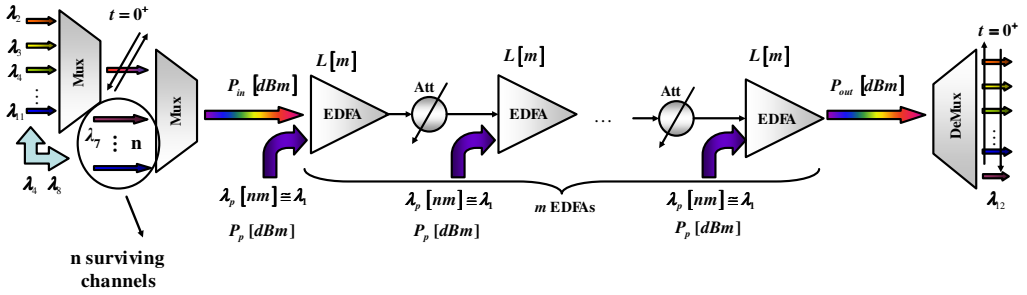

Figure 3-20 *DWDM* simulation setup of an 11:*n* channel drop or a *n*:11 channel add.

Figure 3-18 illustrates a possible optical network link, where a group of n channels are muxed with a previous *DWDM* signal. In this simulation the P_{in} is composed by eleven channels divided into *n* surviving channels and the remaining ones are dropped and added at instant $t=0^+$. Several simulations are performed for an increasing value of *n* and a decreasing value of the dropped/added channels.

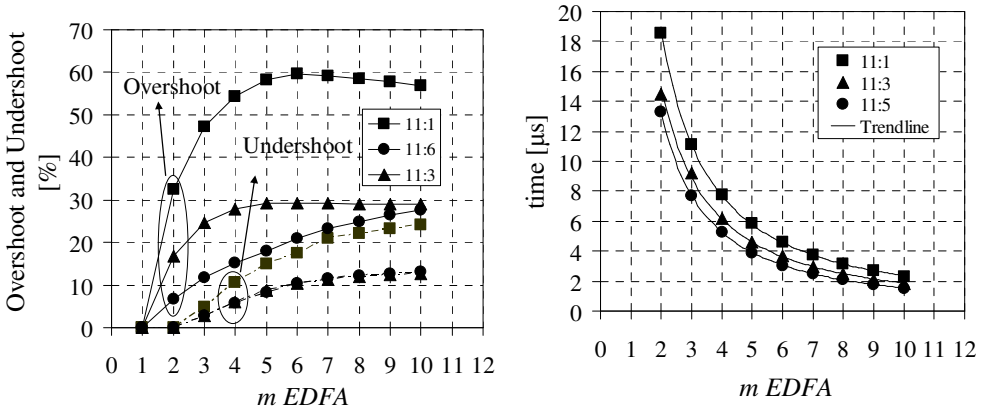

Figure 3-21 Channel drop from 11:*n*: a) Overshoot and undershoot vs. *m EDFA*s b) Peak time vs. *m EDFA*s.

From Figure 3-21 a) is possible to infer that the *Mp*(drop) and *mp*(drop) increases with the increase of the number of channels dropped. From a 6 channel drop to a 10

channel drop, analyzing after ten *EDFA*s, there is an increase of 39% to *Mp* and approximately 7% to *mp*.

Figure 3-21 b) illustrates the peak time. It is possible to infer that the power transient is slower when the number of channel dropped is higher. After ten *EDFA*s, *tp* curves converge to approximately the same value 2 μs. The *tp* curves may be empirically approximated using a power interpolation as:

$$tp(m) \approx \frac{45.8}{m^{1.3}}, \quad 2 \le m \le 10, \quad 11:1\,\text{drop} \quad [\mu s];$$

$$tp(m) \approx \frac{36.9}{m^{1.3}}, \quad 2 \le m \le 10, \quad 11:3\,\text{drop} \quad [\mu s]; \tag{3.19}$$

$$tp(m) \approx \frac{33.5}{m^{1.3}}, \quad 2 \le m \le 10, \quad 11:6\,\text{drop} \quad [\mu s],$$

the variable *m* is the amplifier count. It is interesting to observe that initial condition is higher for an 11:1 drop than for 11:5 drop, which exposes "slower" power transient when n decreases. The power factor is equal on all three expressions of (3.32), which leads to approximation of the three curves with the increase of the *EDFA* count.

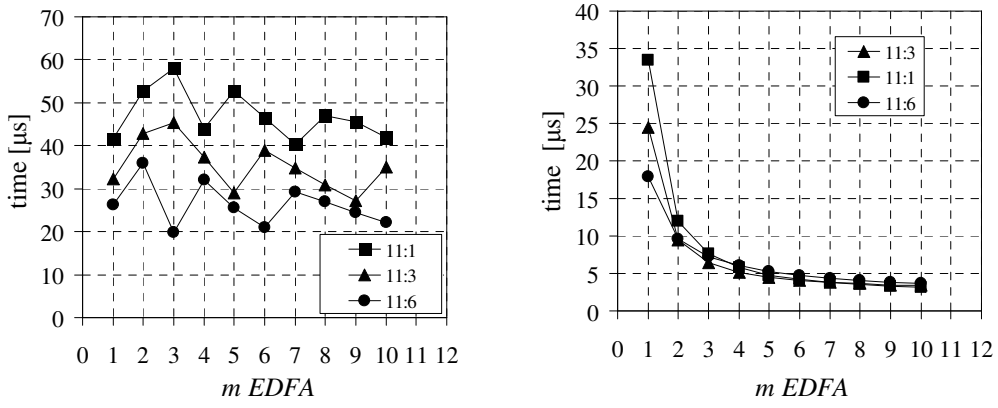

Figure 3-22 Channel drop from 11:*n*: a) Settling time vs. *m EDFA*s b) Rise time vs. *m EDFA*s.

Figure 3-22 exposes settling time (a) and the rise time (b). It is possible to observe that after ten *EDFA*s, 11:1 curve exhibits approximately 43 μs, the 11:3 curve approximately 35 μs and 11:6 curve approximately 22 μs. Although *ts* appears to have

non-linear behaviour with the increase of the number of channels that are dropped is interesting to observe that when five channels are dropped the *ts* has lower values than when ten channels are dropped. When ratio between the number of channels that are dropped and the number of channels in the system is very near to one there is less power available to be distributed by the remaining channels and more channels to which the extra power has to be distributed. Hence, the power transient achieves its vicinity faster when the ratio between the number of channels dropped and the number of channels that compose the *DWDM* signal is near to one than when it is near to zero.

The *tr* after the first *EDFA* exposes (Figure 3-20 b)) a value around 33.4 μs for the 11:1 drop and 17.9 μs for the 11:6 drop. After the third *EDFA* all curves have the approximately same *tr* of 4 μs. With this result is possible to conclude that the impact of variable channel drop has no significant impact, on the time parameters.

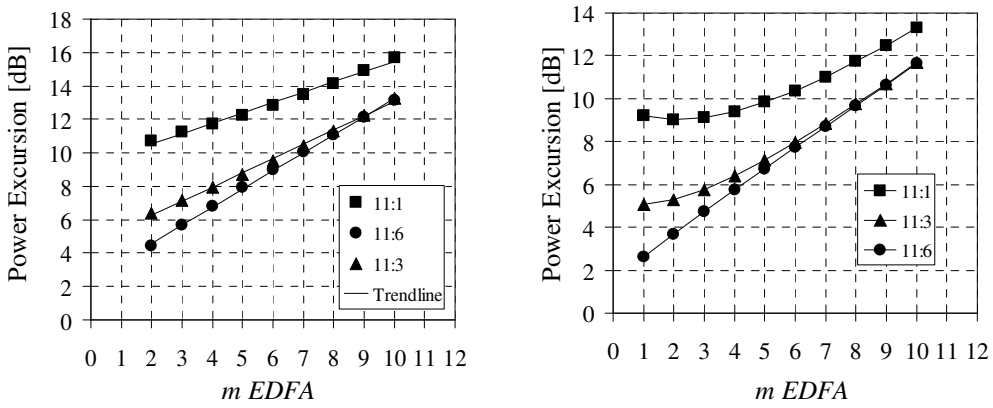

Figure 3-23 Channel drop from 11:*n*: a) Power excursion at *tp* vs. *m EDFA*s b) Power Excursion at *tr* vs. *m EDFA*s.

For Pe_{tp} the increase is empirically approximated using a linear interpolation as:

$$\begin{aligned} Pe_{tp}(m) &\approx 0.6m + 9.3, \quad 2 \le m \le 10, \quad 11:1 \text{ drop} \\ Pe_{tp}(m) &\approx 0.9m + 4.6, \quad 2 \le m \le 10, \quad 11:3 \text{ drop} \quad [dB], \\ Pe_{tp}(m) &\approx 1.1m + 2.4, \quad 2 \le m \le 10, \quad 11:6 \text{ drop} \end{aligned} \tag{3.20}$$

the variable *m* is the amplifier count.

The Pe_{tr} assumes an increasing behaviour, that after ten *EDFA*s presents the same value with a maximum difference of 2dB. The difference between all curves reduces from *EDFA* to *EDFA*. After the first, is possible to observe from Figure 3-23 b) a difference of approximately 6.6 dB and after the tenth all curves exhibit the same value of power excursion. If other channel had been chosen for analysis the power excursion dependency with the number of channels dropped could have a different behaviour

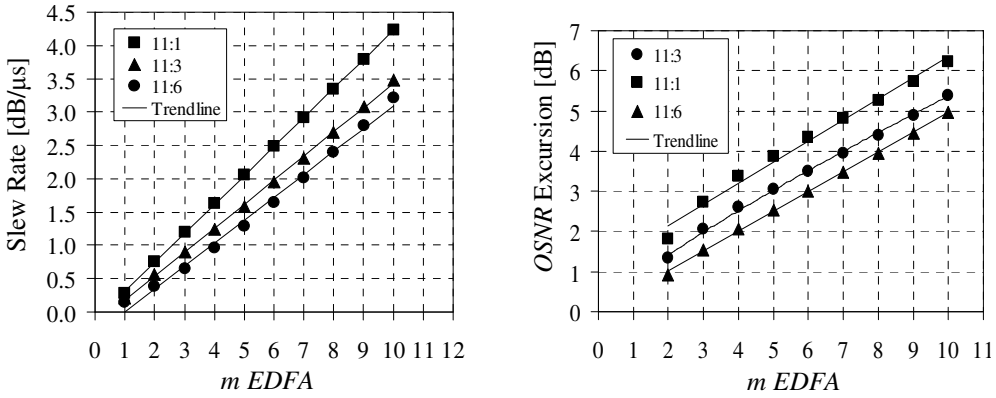

Figure 3-24 Channel drop from 11:*n*: a) Slew Rate vs. *m* of *EDFA*s; b) *OSNR* excursion at instant *tp*.

Figure 3-24 exhibits the slew rate dependency with the *EDFA* count and also with the number of channels dropped. For $SR(m)$ the curves are empirically approximated using a linear interpolation as:

$$\begin{aligned} SR(m) &\approx 0.43m - 0.11, \quad 1 \le m \le 10, \quad 11:1\,\text{drop} \\ SR(m) &\approx 0.36m - 0.20, \quad 1 \le m \le 10, \quad 11:3\,\text{drop} \quad [\text{dB}/\mu\text{s}], \\ SR(m) &\approx 0.35m - 0.43, \quad 1 \le m \le 10, \quad 11:6\,\text{drop} \end{aligned} \tag{3.21}$$

the variable m is the amplifier count. The result exposed on Figure 3-24 b) is empirically approximated using a linear interpolation as:

$$\begin{aligned} OSNR\text{e}(m) &\approx 0.52m + 1.09, \quad 2 \le m \le 20, \quad 11{:}1 \text{ drop} \quad [dB] \\ OSNR\,\text{e}(m) &\approx 0.48m + 0.55, \quad 2 \le m \le 20, \quad 11{:}3 \text{ drop} \quad [dB] \\ OSNR\,\text{e}(m) &\approx 0.49m + 0.02, \quad 2 \le m \le 20, \quad 11{:}6 \text{ drop} \quad [dB] \end{aligned} \quad , \tag{3.22}$$

where *m* is the *EDFA* count. It is possible to infer from Figure 3-24 a) that the requirements are fulfilled until after the second *EDFA*, for the 11:1 and 11:3 curves, and after the third for the 11:6 curve. From Figure 3-24 b) is possible to infer that the peak *OSNR* excursion is above 3dB after the fourth *EDFA* for the 11:1 curve, after the fifth for the 11:3 curve and after the sixth for the 11:6 curve.

3.4 Conclusions

In this section the overall conclusions of the simulations results are presented. The power transient has the following characteristics:

- time parameters are lower when channels added than when channels are dropped, which means that a power transient is faster when channels are added than when channels are dropped.
- time parameters decrease with the increase of the number of *EDFA*s in the chain;
- the difference between a drop and an add, regarding the time parameters, reduces with the increase of the number of *EDFA*s in the chain;
- *tr* and *tp* may be approximated by a power decay;
- *Mp* and *mp* have a similar performance between a channel drop and a channel add;
- overshoot and undershoot converge to a saturation point with the increase of the number of *EDFA*s in the chain;
- *Pe* at *tr* and *tp* instants is similar for a drop and for an add and has an approximately linear behaviour in logarithmic units;
- the slew rate increases with the increase of the number of *EDFA*s in the chain and may be approximated by a linear behaviour.
- *Mp* and *mp* curves decrease with the reduction of $P^{in}_{j,1}$;
- the time parameters remain approximately unchanged with the reduction of $P^{in}_{j,1}$
- the increase rate per *EDFA* remains constant for *Pe* at different instant with an offset decrease of approximate 0.05dB per each 1 dB of $P^{in}_{j,1}$ decrease;
- *SR* experiences a reduction in the increase rate per *EDFA* that is insignificant in terms of network planning;

- the power transient spectral dependency has major impact on the *Pe*, a non-monotonous behaviour depending of which channel is under analysis;
- the overshoot, undershoot and the time parameters are not significantly affected by the *EDFA* gain spectrum;
- an increase of the number dropped/added lead to an growth in the overshoot and undershoot, an increase in the slew rate and in the power excursion parameters;
- time parameters did not present a significant impact with the number of channels dropped.

Chapter 4. Transient in an Optical Link: Experimental Verification

4.1 Introduction

This chapter presents an experimental study of power transient effect in amplifier chains. It intends to complement the simulation study presented in chapter 3. It will be shown that the behaviour observed previously for the transient parameters like transition time and overshoot are in fact, verified by experiment. The chapter starts with section 4.2 where a two-channel *WDM* setup is used to analyze the parameters defined in section 2.2. In section 4.3 one of the two-channel *WDM* signal is replaced by an eleven-channel *DWDM* signal. The conclusions are presented in section 4.4.

4.2 Transient in an *EDFA* chain with continuous wave signals

In the first experiment two channels have been used. *CW* channels have been tuned at several locations:

Ch #	**1**	**2**	**3**	**4**	**5**	**6**	**7**	**8**	**9**
[nm]	1546.8	1547.6	1548.4	1549.2	1550	1550.8	1551.6	1552.4	1553.2

Table 3- *CW* wavelengths used in experimental verification with 0.8 nm spacing.

The experience was conducted according to setup of Figure 4-1.The first external cavity laser (*ECL* 1) is tuned into Ch 5 and is switched on, continuously. The second ECL is modulated with a Mach-Zhender (*MZ*) interferometer and tuned at different channel wavelengths with a spacing of 0.8 nm, which corresponds to a spacing of 100 GHz. Thus, a typical *DWDM* grid is emulated. After passing through the *MZ*, the power from the second laser is modulated into a rectangular wave with a defined period of 400 µs, simulating a 200 µs power step (add/drop). In this setup variable optical attenuators (*VOA*) are used to maintain the same input power in all *EDFA*s. The importance of the optical spectral analyzer (*OSA*) in this setup comes from the need of assure the same input power for both laser signals (-15 dBm/Ch). The number

of *EDFA*s (*m*) is variable between 1 and 5 amplifiers in cascade. A passband filter is used to separate the surviving signal from the modulated signal previously multiplexed by the coupler.

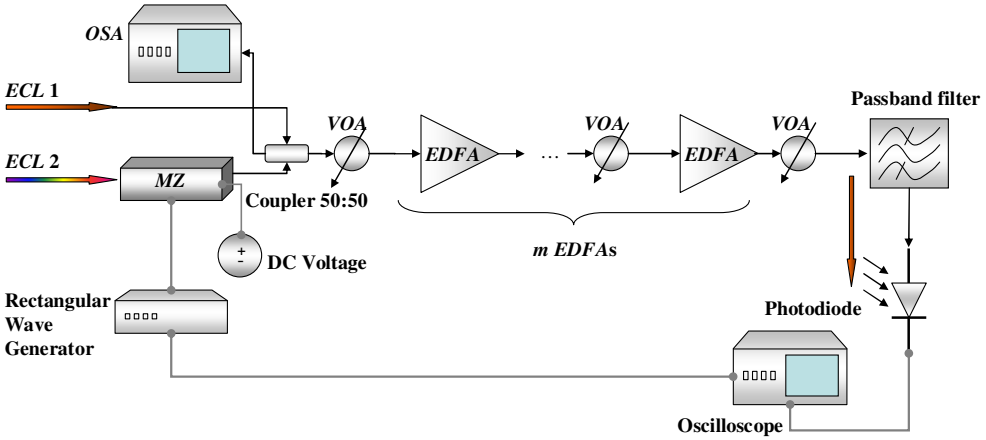

Figure 4-1 Experimental setup for power transient analysis in a cascade of *m EDFA*s.

The transient response after 1 *EDFA* visualized on the oscilloscope by Ch 5, using the second laser tuned at Ch 6, is displayed on Figure 4-2.

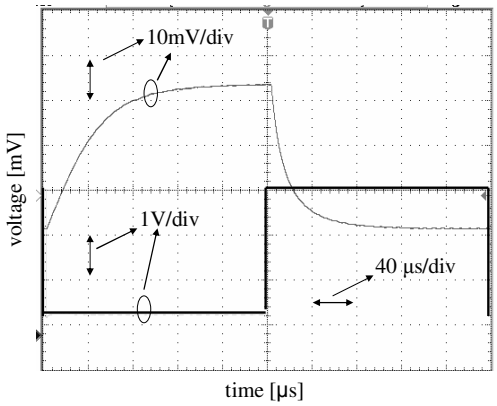

Figure 4-2 Transient response after 1 *EDFA* with -15dBm/Ch; Ch5: 1550 nm (in picture); Ch6: 1550.8 nm (modulated).

From Figure 4-2 it is possible to qualitatively, observe as expected from simulation, illustrated on Figure 2-19 and 2-20, a first order system response. When the power from Ch 6 decreases, simulating a channel drop, the power of Ch 5 increases. Thus, the expected behaviour from the simulation analysis is demonstrated with the occurrence of a power excursion. On the other hand, when the power from Ch 6 increases (emulating a channel add) the power on Ch 5 decays.

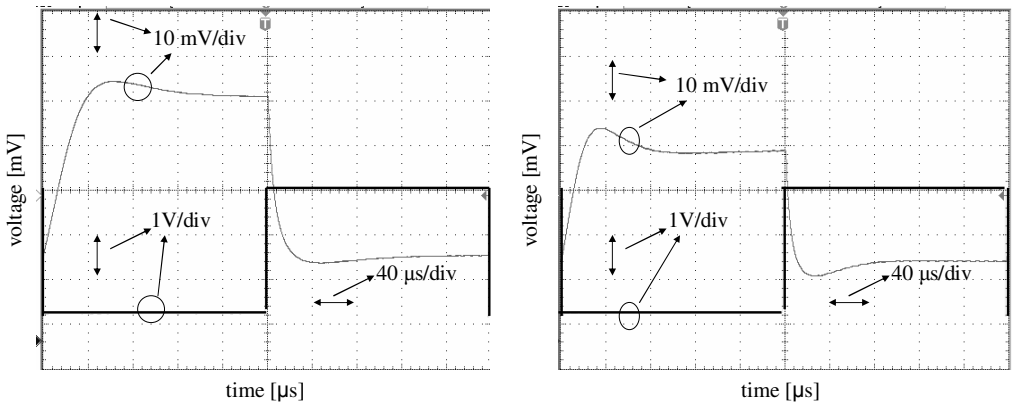

Figure 4-3 Transient response after 2 *EDFA*s (a) and after 3 *EDFA*s (b) with -15 dBm/Ch; Ch5 in picture and Ch6 modulated.

After the second *EDFA* the Ch 5 power transient response to add and drop of Ch 6 acquires a second order oscillatory response. The increasing number of *EDFA*s in the chain significantly decreases the rise time, causing much faster transients and also an increase of overshoot and undershoot, as it is possible to infer from Figure 4-4, which presents power transients after four and five *EDFA*s respectively.

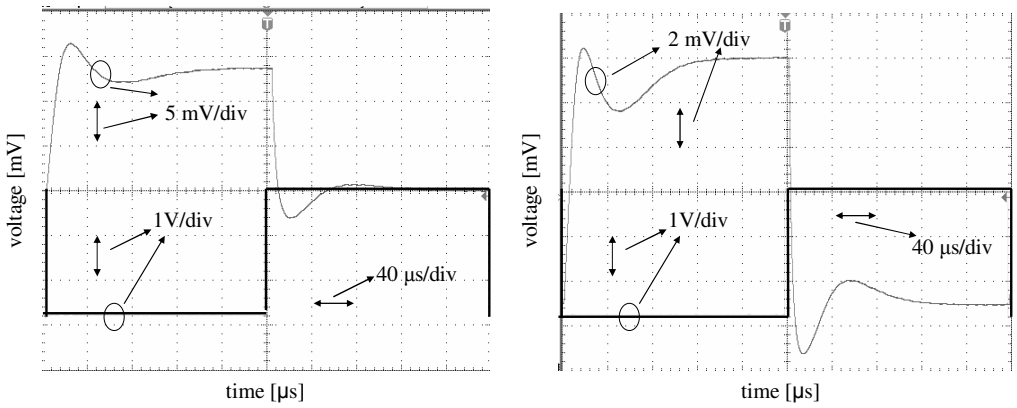

Figure 4-4 Transient response after 4 *EDFA*s (a) and after 5 *EDFA*s (b) with -15dBm/Ch; Ch5 in picture and Ch6 modulated.

These results are according to the simulations presented in section 3.2 . In order to have a quantitatively vision of transients, is important to expose the experimental results according to the parameters defined in section 2.2.

Figure 4-5 exposes the rise time and fall time dependence with the number of *EDFA*s in the chain. Rise time of Ch5, *tr*, when Ch6 is dropped after the first *EDFA* is approximately of 80µs. *tr* decays with the increase of the *EDFA* count. After the

second *EDFA* is of 30 µs, which means the power transient of Ch5 became faster in 50µs.

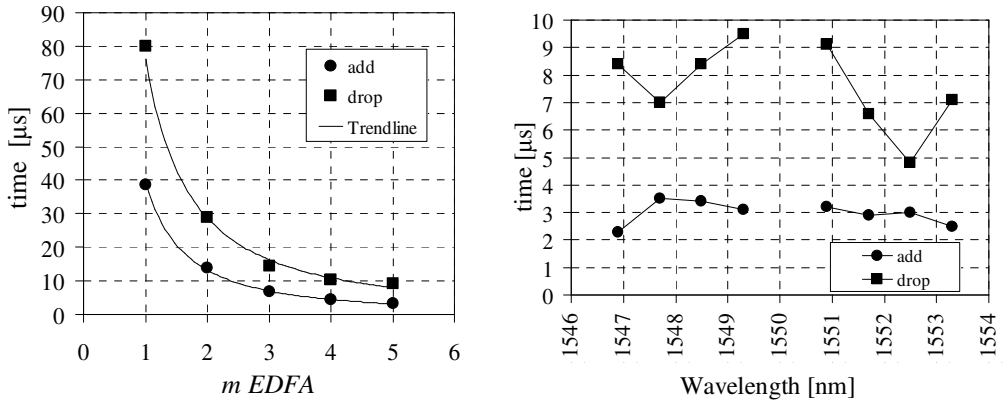

Figure 4-5 Ch5 in picture and Ch6 modulated with -15 dBm/Ch: a) Rise and Fall time (*tr*) vs. *m EDFA*s; b) Rise and Fall time (*tr*) vs. Wavelength for Ch5 after 5 *EDFA*s.

In addition, the third *EDFA* decreases the rise time in 15µs, and after the fourth *EDFA* the rise time is of 10µs and the decrease with the addition of one more *EDFA* (5 *EDFA*s) is just of 1µs. Thus, after the fourth *EDFA* the rise time of the transient does not decrease significantly, being the main contributions from the first three *EDFA*s. The fall time (add), *tr*, has also a decay behaviour. The expected faster behaviour of adding channels is clear from Figure 4-5 a). In fact, the transient is faster when channels are added than when channels are dropped. After the first *EDFA* *tr* has a fall time of 40µs, which is a difference of more or less 40µs from the rise time of drop. After the second *EDFA* the decrease on *tr* is of approximately 25µs, which is less than the same situation for the rise time. The decay curve of the fall time is less abrupt but is always below the rise time curve, which means the transient is faster after all *EDFA*s. After the fourth *EDFA* the fall time does not increase significantly, more or less 1µs, and there is difference of 5µs between rise time and fall time. The *tr* (drop) curve may be empirically approximated using a power interpolation as:

$$tr(m) \approx \frac{76.1}{m^{1.4}}, \quad 1 \le m \le 5, \quad [\mu s], \tag{4.1}$$

where, *m* is the amplifier count. In the case of channel add, this relation becomes:

$$tr(m) \approx \frac{39.3}{m^{1.6}}, \quad 1 \le m \le 5, \quad [\mu s]. \tag{4.2}$$

Figure 4-5 b) exhibits the Ch5 power transient dependency with the wavelength of the channel dropped/added after a chain of 5 *EDFA*s. It is possible to infer from the results that the relationship between the transition time of Ch5 and the wavelength of the channel dropped/added is non-monotonous, enhancing the non-linear behaviour of transients. However, when channels are added the *tr* variations are inferior to 2 μs, between 4 μs and 2 μs, and when channels are dropped the *tr* variations have approximately 4.3 μs maximum, inferior to 9.1 μs and above 4.8 μs.

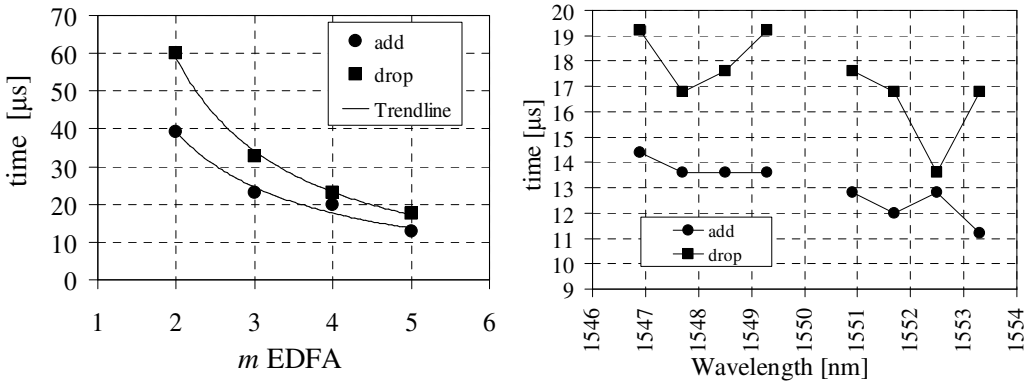

Figure 4-6 Ch5 in picture and Ch6 modulated with -15 dBm/Ch: a) Peak time (*tp*) vs. *m EDFA*s; b) Peak time (*tp*) vs. Wavelength for Ch5 after 5 *EDFA*s.

Figure 4-6 a) illustrates the peak time dependency with the *EDFA* count. It is possible to infer a decrease on peak time with the number of *EDFA*s in the chain. Since the transient after the first *EDFA* is a first order system response, there is no peak time.

After the second *EDFA* the transient has a peak time of 60μs for the drop and 40μs for add, computing a difference of 20μs between a drop and an add channel scenario. The difference reduces with the number *EDFA*s. After the third *EDFA tp* is 33μs and 23μs for add and drop respectively. The *tp* (drop) curve may be empirically approximated using a power interpolation as:

$$tp(m) \approx \frac{147.9}{m^{1.3}}, \quad 2 \le m \le 5, \quad [\mu s], \tag{4.3}$$

where, *m* is the amplifier count. In the case of channel add, this relation becomes:

$$tp(m) \approx \frac{86.5}{m^{1.1}}, \quad 2 \le m \le 5, \quad [\mu s]. \tag{4.4}$$

Expressions (4.1) to (4.4) provide a simple estimate of the *tr* and *tp* variation with the number of amplifiers in the chain.

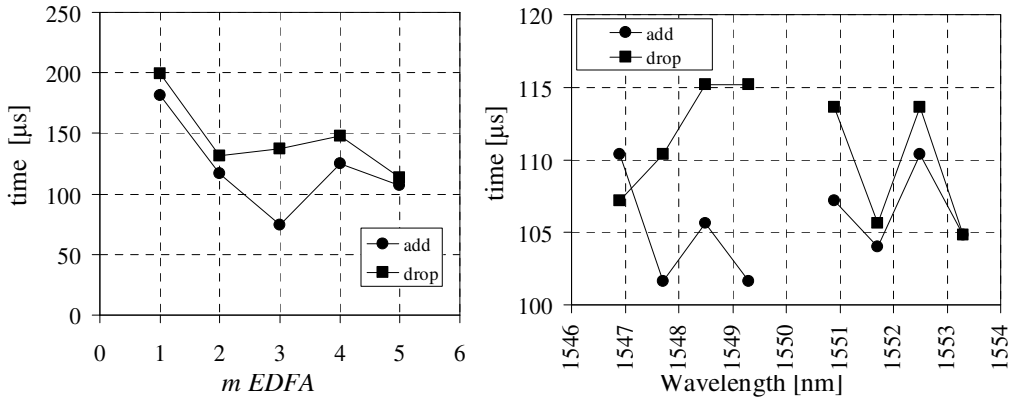

Figure 4-7 Ch5 in picture and Ch6 modulated with -15 dBm/Ch: a) Settling time (*ts*) vs. *m EDFA*s; b) Settling time vs. Wavelength after 5 *EDFA*s (Ch5 in picture and *ECL2* varible).

Settling time (*ts*), due to definition, is difficult to measure the instant in time the system achieves the new set point with a margin of 2%, thus the error associated to this measure is high. From Figure 4-7 it is not possible to establish a tendency for settling, but a decrease was expected and has a similar qualitatively behaviour than the exposed on Figure 3-3 b) simulation. Settling time, *ts,* has an oscillatory behaviour. After a variable number of *EDFA*s, *ts* increases due to power transient oscillatory behaviour, some oscillations that were inferior to 2% become higher resulting in *ts* increases. There is clear non-linear dependency with the wavelength of the drop/add signal as is illustrated on Figure 4-7 b).

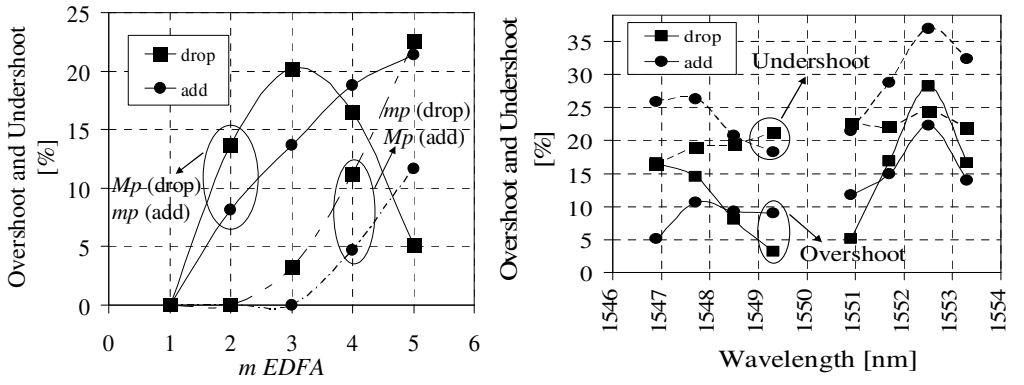

Figure 4-8 Ch5 in picture and Ch6 modulated with -15 dBm/Ch: a) Overshoot and Undershoot vs. *m EDFA*s

From Figure 4-8 the overshoot, *Mp* (drop), exposes a maximum achievement after the third *EDFA*. This behaviour was already observed in Figure 3-11 a) simulation. However, *mp* (add) typically has a similar behaviour than *Mp* (drop), in this experience that did not happen. It is important to remember that for simulation the *ASE* was not considered and in experience it can saturate the *EDFA*s.

4.3 Transient in an *EDFA* chain with a *DWDM* signal

In the second experiment eleven wavelengths have been used. A *CW* channel has been tuned at Ch 11. A *DWDM* signal has been multiplexed according to Table 4.

Ch #	1	2	3	4	5	6	7
[THz]	195.9	195.5	195.1	194.7	194.3	193.9	193.5
[nm]	1531.39	1534.53	1537.67	1540.83	1544.00	1547.19	1550.39

Ch #	8	9	10	11
[THz]	193.1	192.7	192.3	191.9
[nm]	1553.60	1556.82	1560.06	1562.23

Table 4 Modulated commercial available tunable wavelength lasers used in experimental verification with 400 GHz spacing.

The experience was conducted according to setup of Figure 4-9. The first external cavity laser (*ECL* 1) is tuned into Ch 11 and is switched on, continuously. An arrayed waveguide grating (*AWG*) is used to multiplex *N* modulated wavelengths. The

resulting total power of the *DWDM* signal is modulated into a square wave with a defined period of 400 µs, simulating a 200 µs power step (add/drop).

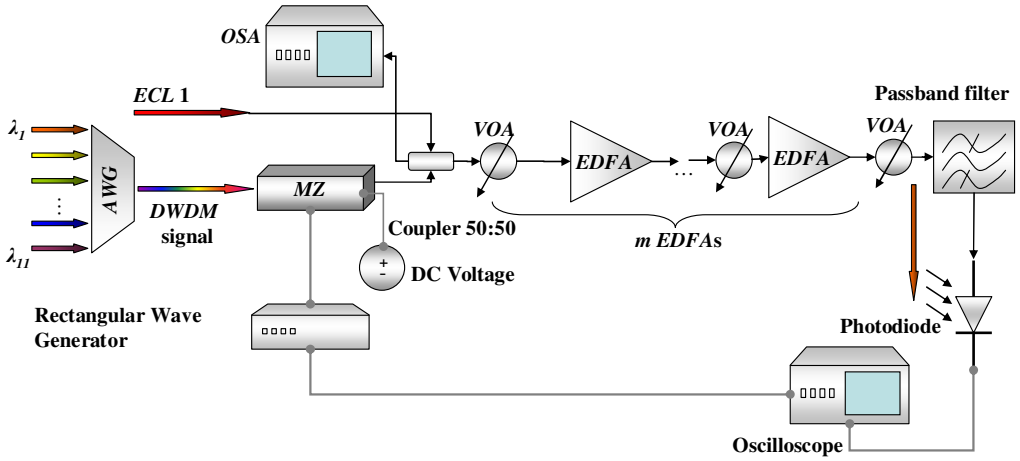

Figure 4-9 Experimental setup for power transient analysis in a cascade of *m EDFA*s with a *DWDM* signal.

In this setup the same input power is also applied to all *EDFA*s (-15 dBm/Ch). The number of *EDFA*s (*m*) is variable between 1 and 5 amplifiers in cascade. A passband filter is used to separate the surviving signal from the modulated signal previously multiplexed by the coupler. In a first scenario the lasers are tuned according to Table 4. Hence, the *DWDM* signal is composed by ten channels, λ_1 = Ch1 to λ_{10} = Ch10, plus one *CW* channel, tuned at λ_{11}.

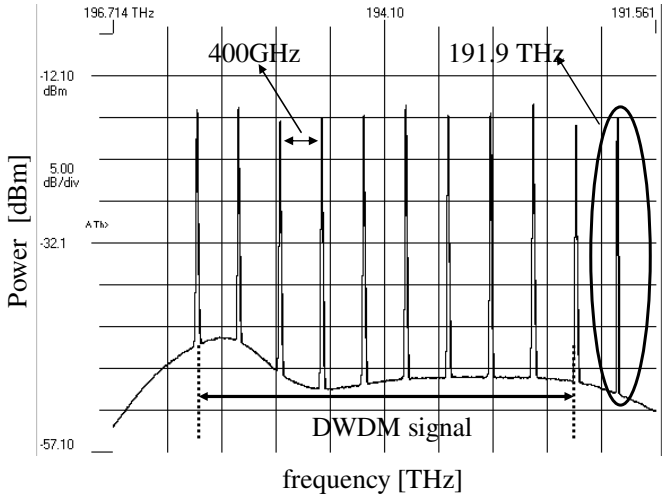

Figure 4-10 *DWDM* signal spectrum with -15 dBm/Ch and 400GHz spacing (ITU-T Grid).

All channels are spaced of 400 GHz, according to what is illustrated on Figure 4-10. As has been said before, *EDFA*s do not distribute the gain equally for all channels.

Thus, variable optical attenuators were used to after the *AWG* in order to equalize (as much as possible) the signals. From Figure 4-10 is possible to observe small power fluctuations between channels which outcome from the *MZ* sensitivity to signal polarization that changes with fiber bends and oscillations. Hence, channels drop/add from 11:1 and 1:11 respectively, is simulated in a first experience.

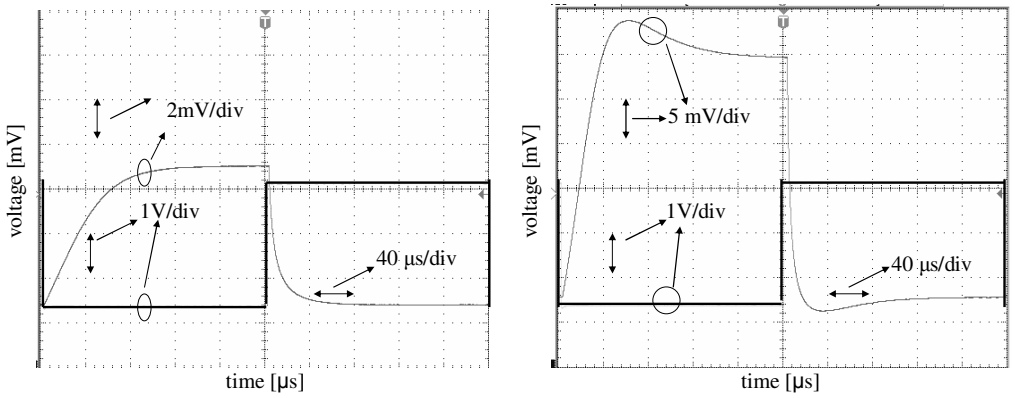

Figure 4-11 Power transient of Ch 11 after a) 1 *EDFA*; b) 2 *EDFA*s.

From Figure 4-11 to Figure 4-13 the power transient is after 1 *EDFA* to 5 *EDFA*s respectively is exposed.

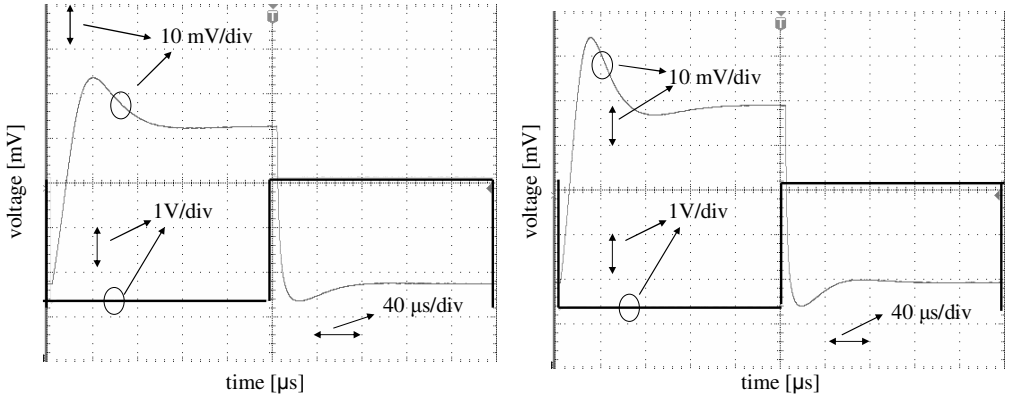

Figure 4-12 Power transient of Ch 11 a) 3 *EDFA*s ; b) 4 *EDFA*s.

Is possible to observe a similar behaviour to the one obtained on the two channel experiment. After the first *EDFA* the power transient does not expose overshoot or undershoot. After the second *EDFA* the overshoot and undershoot becomes visible on the drop and on the addition of 11 channels, respectively.

The overshoot and undershoot becomes more prominent from *EDFA* to *EDFA*. There is also a decrease on the rise and the fall number with the number of *EDFA*s. The fall time, *tr*(add), also has smaller values than the rise time, *tr*(drop).

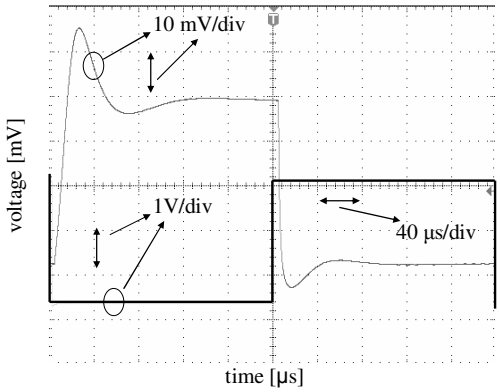

Figure 4-13 Power transient of Ch 11 after 5 *EDFA*s.

The evolution of *tr* with the number of *EDFA*s on the optical link is exposed on Figure 4-14 a) and the evolution of *tp* is illustrated on Figure 4-14 b). The *tp* also expose a similar behaviour to the one exposed on Figure 4-6, which *tp* (add) presents smaller values than *tp* (drop). Comparing the results obtained on the two different experiments, the power transient response is faster in *DWDM* scenario than in a two channel scenario. This result is congruent to the results obtained by simulation, which lead to the same conclusion. However, after five *EDFA*s *tr* (drop) and *tr* (add) converge to a value of approximately 9 µs and 2 µs respectively, according to Figure 4-14 a). Figure 4-14 b) illustrates the experimental result for *tp* dependency with the number of *EDFA*s in cascade. After five *EDFA*s, *tp* (drop), converges to approximately 26 µs and *tp* (add) converges to 13 µs.

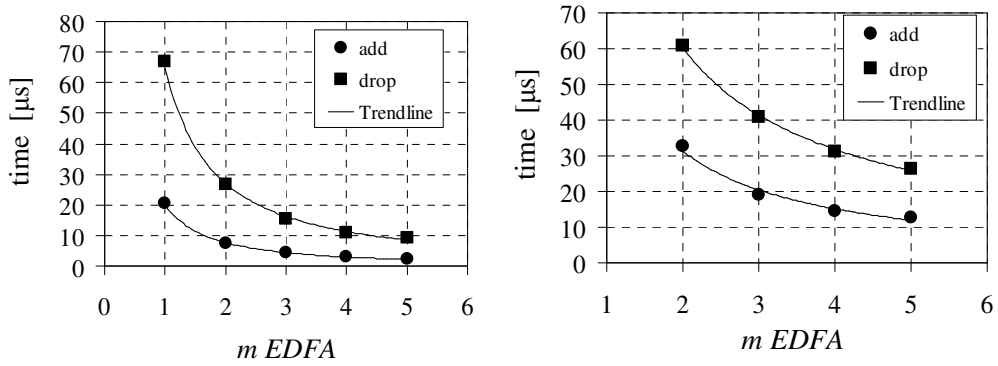

Figure 4-14 An 11:1 channel drop and an 1:11 channel add: a) Rise/Fall Time vs. *m EDFA*s b) Peak Time vs. *m EDFA*s.

The *tr* (drop) curve may be empirically approximated using a power interpolation as:

$$tr(m) \approx \frac{64.8}{m^{1.3}}, \quad 1 \le m \le 5, \quad [\mu s], \tag{4.5}$$

where, *m* is the amplifier count. In the case of channel add, this relation becomes:

$$tr(m) \approx \frac{19.9}{m^{1.4}}, \quad 1 \le m \le 5, \quad [\mu s]. \tag{4.6}$$

The *tp* (drop) curve may be empirically approximated using a power interpolation as:

$$tp(m) \approx \frac{113.5}{m^{0.9}}, \quad 2 \le m \le 5, \quad [\mu s], \tag{4.7}$$

where, *m* is the amplifier count. In the case of channel add, this relation becomes:

$$tp(m) \approx \frac{64.6}{m^{1}}, \quad 2 \le m \le 5, \quad [\mu s]. \tag{4.8}$$

It is interesting to note that, although the transitions area faster in the 11 channel case, the rate decay of the transition time with the amplifier count is lower than the two-channel case.

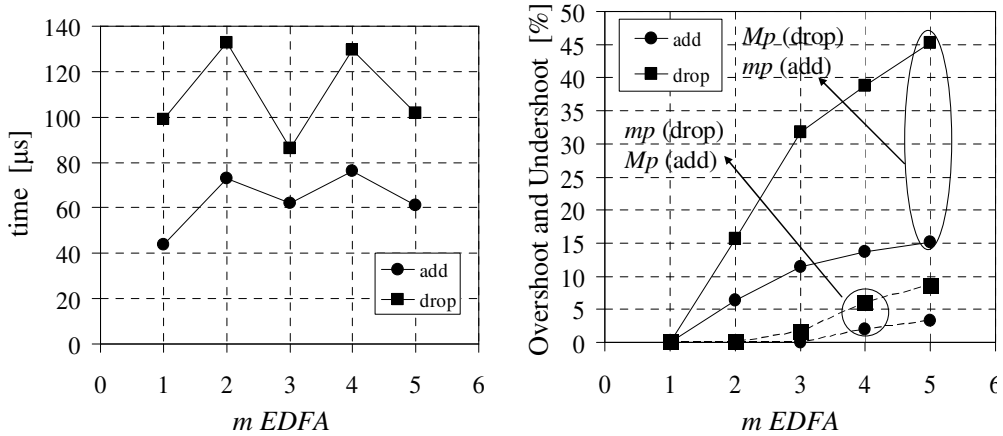

Figure 4-15 An 11:1 channel drop and an 1:11 channel add: a) Settling time vs. *m EDFA*s; b) Overshoot and Undershoot vs. *m EDFA*s.

Settling time (*ts*), as is illustrated on Figure 4-15, exposes an oscillatory behaviour, as was expected by simulation scenario described in section 3.3 and illustrated on Figure 3-11 b).

The dependency of the overshoot with amplifier count Figure 4-15 b) shows substantial increase with respect to the 2-channel system. This increase results from a higher power fluctuation at the input of the amplifier chain. Nevertheless, one must note that, in the case of a channel drop, the overshoot of the channel under analysis is never high enough to saturate the amplifier and reduce the overshoot, as observed in the 2 channel system. This effect would certainly occur for a higher amplifier count.

4.4 Conclusions

The experimental results show that the power transient response match with the reasonable approximation to a second order response after the second *EDFA* and a first order response after the first *EDFA*, as proposed initially. It has been shown that the overshoot of the transient is closely related to the saturation power of the *EDFA*s and may follow a non-monotonic dependency with the amplifier count, result that has been also exhibit through the simulation section. Furthermore, empirical expressions are proposed to describe the dependency of the transition time on the amplifier count. Quantitatively, it is shown that, for the considered amplifiers, the transition time for a drop event decreases with a power factor of 1.4 whereas for an add event this factor is increased to 1.6. Additionally, the experiment is extended to an 11 channel system. In this case, it is shown that the transition times for drop and add events are reduced, following a power factor of 1.3 and 1.4, respectively. This shows that by increasing the channel count, and consequently, the magnitude of the power transition, the transient becomes faster. However, the rate of decrease of transition time becomes lower.

Chapter 5. Conclusions

In this chapter the focus of this report is summarized and main conclusions are presented in section 5.1 and follows section 5.2 where proposals for future work are presented.

5.1 Summary and Main Conclusions

The work reported in this thesis focus the topic of power transients on reconfigurable optical networks. Nowadays, this architecture starts to become commercial available and deployed in optical transport networks, promising to become more commonplace in a near future. The growth in traffic demands and variable bandwidth needs combined with the growth of all-optical networks will enhance the power transient's impact on the network optical performance which fully motivated the present study.

An exhaustive study of the *EDFA* intrinsic characteristics and on previous work that had been done on power transients was carried out. The aim of this analysis was to better understand the *EDFA* behaviour that leads to power transients and which analytical models were common used for an *EDFA* dynamic approach.

In order to evaluate the optical performance of a link a simulation methodology was chosen and, therefore, an *EDFA* analytical dynamic model was implemented, an "instantaneous" noise model for chains of *EDFA*s was developed as also the analytical model of a *PIN* receiver. MATLAB programming language was chosen, since it was considered to be the most suitable. Several experiences were performed, which corroborated the simulation results.

This work has shown that a power transient may be characterized in a simple manner using some parameters for a second order response. In particular, the transition time

and the overshoot. Simplified rules have been proposed to define acceptable limits for the transient time and overshoot of a power transient. Quantitatively, these rules are a maximum 26% of overshoot in case of a channel drop or fiber break due to fiber nonlinearities; maximum 3dB of *OSNR* variation to avoid excessive *BER* and ensure a maximum *BER* for *FEC* operation. A maximum transient slew rate of 0.5dB/μs, to ensure effective response of the *AGC* in the optical receiver. Output power per channel range between -13 dBm and 4 dBm, to ensure operation with power levels above the sensitivity and bellow the overload thresholds. This last parameter is applied in optical networks with *EDFA*s with gain control mechanism that force the output power to be within -13 dBm and 4 dBm, in *EDFA*s with constant pump power the ouput power in steady state can be above 4 dBm.

These parameters severely limited the number of *EDFA*s cascaded. This work shows a limitation of 7 *EDFA*s due to slew rate after a channel is added in a two-channel scenario and a 12 *EDFA* limitation after a drop. A maximum of 10 *EDFA*s cascaded to ensure a 3dB of maximum *OSNR* fluctuations. Thus, in order to avoid performance degradation of the optical link it is crucial to suppress the transient response by the use of transition suppression thecnics. The reduction of the input power per channel at the input of the first *EDFA* of the optical link, with constant attenuation, leads to a reduction in the overshoot but the time parameters remain unchanged. The overshoot is limited by the output saturation power. The experimental results have shown, qualitatively, the same behaviour obtained by simulation. The power transient can be characterized using second order behaviour time parameters. These rise and peak time parameters may be approximated using power decays.

5.2 Future Work

The research developed throughout the course of this work enabled the identification of several possible avenues for further investigation. Among these, the following are considered to be the most relevant:

- The study of reduced transients rules for optical network planning.

- The study of transient suppression thecniques.
- Develop a *BER* model based on the study of several optical receivers with experimental verification.

References

[1] Borella,M., Jue,J., Banerjee,D., Ramamurthy,B. and Mukherjee,B., "Optical Components for WDM Lightwave Networks", *Proceedings of the IEEE*, Vol. 85 No. 8, August 1997, pp. 1274-1307.

[2] Desurvire,E., "*Erbium-Doped Fiber Amplifiers: Principles an Applications*", John Willey & Sons, Inc. 1994.

[3] Agrawal,G., "*Fiber-Optic Communications Systems*", John Willey & Sons, Inc.2002.

[4] Ramaswami,R., Sivarajan,K., "*Optical Networks: A practical perspective*", Morgan Kaufmann editors, San Francisco, EUA, 2002.

[5] Bracket,C., "Dense Wavelength Division Multiplexing Networks: Principles and Applications", *IEEE J. Select. Areas Commun.*, August 1990, Vol. 8, No. 6, pp. 948-964.

[6] Iannone,E., Sabella,R., "Optical Path Technologies: A Comparison Among Different Cross-Connect Architectures", *Journal of Lightwave Technology*, Vol. 14, No. 10, October 1996, pp. 2184-2196.

[7] Kaminow,I., Li,T., "Optical Fiber Telecommunications IVB: Systems and Impairments", Chap. 8, *Academic Press*, EUA, 2002.

[8] Hayee,M., Willner,A., "Transmission Penalties Due to EDFA Gain Transients in Add-Drop Multiplexed WDM Networks", *IEEE Photonics Technology Letters*, July 1999, Vol. 11, no.7, pp. 889-891.

[9] Kim,S., Chung,J., Lee,B., "Optical Amplifiers and Their Applications", *OSA Trends in Optics and Photonics Series*, Washington, DC: Opt. Soc. Amer., 1997, Vol. XVI, paper MC5.

[10] Ben-Ezra,Y., Haridim,M., Lembrikov,B., "All-Optical AGC of EDFA Based on SOA", *IEEE Journal of Quantum Electronics*, December 2006, Vol. 42, pp. 1209-1214.

[11] Bononi,A., Rusch,L., "Doped-Fiber Amplifier Dynamics: A System Perspective", *IEEE Journal of Ligthwave Technology*, May 1998, Vol. 16, pp. 945-956.

[12] Tian,C., Kinoshita,S., "Analysis and Control of Transient Dynamics of EDFA pumped by 1480 and 980 nm lasers", *Journal of Lightwave Technology*, August 2003, Vol. 21, No. 2, pp. 1728-1734.

[13] Luo,G., Zyskind,J., Nagel,J., Ali,M., "Experimental and Theoretical Analysis of Relaxation-Oscilations and Spectral Hole Burning Effects in All-Optical Gain-Clamped EDFAs for WDM Networks", *Journal Lightwave Technology*, April 1998, Vol. 16, No. 4, pp. 527-533.

[14] Mecozzi,A., Marcenac,D., "Theory of Optical Amplifier Chains", *Journal Ligthwave Technology*, May 1998, Vol. 16, No. 5, pp. 745-756.

[15] Sun,Y., Zyskind,J., Srivastava,A., "Average Inversion Level, Modeling, and Physics of Erbium-Doped Fiber Amplifiers", *IEEE J. Sel. Topics Quantum Electron.*, 1997, Vol. 3, pp. 991-1007.

[16] Karázek,M., "Optical Amplifiers in Dynamic Networks with All-Optical Routing", *IEEE ICTON 2002*, Mo.C.3, pp. 57-61.

[17] Ko,K., Demokan,M., "Transient Analysis of Erbium-Doped Fiber Amplifiers", *IEEE Photonics Technology Letters*, December 1994, Vol. 6, No. 12, pp. 1436-1438.

[18] Sun,Y., Luo,G., Zyskind,J., Saleh,A., Srivastava,A., Sulhoff,J., "Model for Gain Dynamics in Erbium-Doped Fibre Amplifiers", *IEEE Electronics Letters*, August 1996, Vol.32, No.16, pp. 1490-1491.

[19] Srivastava,A., Sun,Y., Zyskind,J., Sulhoff,J., "EDFA Transient Response to Channel Loss in WDM Transmission System", *IEEE Photonics Technology Letters*, March 1997, Vol. 9, No.3, pp. 386- 388.

[20] Franklin,G., Powell,J., Emami-Naeini, A., "Feedback Control of Dynamic Systems", Prentice-Hall Inc. 2002, Fourth Edition.

[21] Sun,Y., Srivastava,A., Zyskind,J., Sulhoff,J., Wolf,C. and Tkach,R., "Fast-Power Transients in WDM optical networks with cascaded EDFAs", *Electronic Letters*, February 1997, Vol. 33, No.4, pp. 313-314.

[22] Otani,T., Goto,K., *et al.,* "Effect of Span Loss Increase on the Optically Amplified Communication System", *Journal of Lightwave Technology*, May 1997, Vol. 15, No. 5, pp. 737-742.

[23] Wong,W., Tsai, H. *et al.*, "Novel Time-Resolved Measurements of Bit – Error-Rate and Optical-Signal-to-Noise-Ratio Degradation due to EDFA Gain Dynamics in a WDM Network", *Optical Fiber Communications*, 2002, pp. 515-516.

[24] J. Elbers, A. Fäbert, C. Scheerer, C. Glingener, and G. Fischer, "Reduce model to describe SPM-limited fiber transmission in dispersion-managed lightwave systems", *IEEE J. Sel. Topics Quantum Electron.*, March/April 2000, vol. 6, no. 2, pp. 276-281.

[25] Paiva,C., "Fibras Amplificadoras Dopadas com Érbio", *Departamento de Engenharia Electrotécnica e de Computadores,* IST Março 2002.

[26] Pachincke,S., Krummrich,P., Voges,E., Gottwald,E., "Transient Gain Dynamics in Long-Haul Transmission Systems with Electronic EDFA Gain Control", *Journal of Optical Networking*, September 2007, Vol. 6, No.9, pp. 1129-1137.